A new depositional model for glaciogenic Neoproterozoic iron formation: insights from the chemostratigraphy and basin configuration of the Rapitan iron formation[1]

Geoffrey J. Baldwin, Elizabeth C. Turner, and Balz S. Kamber

Abstract: Neoproterozoic iron formations record an unusual and apparently final recurrence of this sediment type after a hiatus of more than one billion years. Despite the unusual environmental conditions that led to their formation, specifically their association with glaciogenic deposits, Neoproterozoic iron formations have strongly influenced models for the Precambrian Earth's surficial evolution and iron formation in general. A suite of high-quality trace element data for 42 samples from the Rapitan iron formation in northwestern Canada were used to reconstruct the configuration and redox evolution of the Rapitan Basin. Complete rare-earth element and yttrium (REE+Y) patterns demonstrate that the Rapitan Basin was hydrologically connected to the open ocean, but that local catchments of an evolved, possibly granitic composition supplied dissolved REE+Y, suggesting partial basin restriction. Molybdenum and U systematics are consistent and indicate a partly restricted, or "silled" basin. In contrast to modern analogues for such basins, such as the Cariaco Basin, the stratigraphic association with glaciogenic clastic rocks requires ice cover to be considered in basin reconstruction. Accordingly, the Rapitan iron formation was deposited through a complex interplay of processes: during intervals of ice cover, glacially sourced iron oxyhydroxides were bacterially reduced to dissolved ferrous iron, which was subsequently oxidized to ferric iron following ice withdrawal. During this time, extreme primary productivity in the shallow water column drove eutrophication at middle water depths and the production of a three-tiered stratified water column with ferruginous deep water, a thin euxinic wedge at middle depths, and oxic surface water. Regardless of the basinal redox conditions and depositional constraints, the absence of a positive Eu anomaly in the Rapitan iron formation suggests that the global ocean was fully oxygenated by the Neoproterozoic.

Résumé : Des formations de fer datant du Néoprotérozoïque enregistrent une récurrence inhabituelle et apparemment finale de ce type de sédiment après un hiatus de plus d'un milliard d'années. Malgré les conditions environnementales inhabituelles qui ont mené à leur formation, en particulier leur association avec les dépôts d'origine glaciaire, les formations de fer du Néoprotérozoïque ont fortement influencé les modèles de l'évolution de la surface de la Terre au Précambrien et les formations de fer en général. Un ensemble de données de grande qualité d'éléments traces pour 42 échantillons de la formation de fer de Rapitan dans le nord-ouest du Canada a été utilisé pour reconstruire la configuration et l'évolution redox du bassin Rapitan. Des patrons complets d'éléments de terres rares + Y démontrent que le bassin Rapitan était hydrologiquement relié au grand large, mais que des bassins hydrologiques locaux de composition évoluée, possiblement granitique, ont fourni des éléments de terres rares + Y dissous, suggérant une restriction partielle du bassin. La systématique du molybdène et de l'uranium est constante et indique un bassin partiellement restreint ou « avec seuil ». Contrairement aux analogues modernes pour de tels bassins, par exemple le bassin Cariaco, l'association stratigraphique avec des roches clastiques d'origine glaciaire demande de tenir compte d'une couche de glace lors de la reconstruction du bassin. Par conséquent, la formation de fer Rapitan a été déposée par une interaction complexe de processus : durant des intervalles de couverture de glace, des oxy-hydroxydes de fer, de provenance glaciaire, ont été réduits, par des bactéries, en fer ferreux dissous, lequel a par la suite été oxydé en fer ferrique après le retrait des glaces. Durant ce temps, une extrême productivité primaire dans l'eau peu profonde a poussé l'eutrophisation jusqu'à des profondeurs d'eau moyennes et a produit une colonne d'eau stratifiée à trois étages avec de l'eau ferrugineuse en profondeur, une mince tranche euxinique à une profondeur moyenne et de l'eau oxique en surface. Sans égards aux conditions redox du bassin et aux contraintes de déposition, l'absence d'une anomalie Eu positive dans la formation de fer Rapitan indiquerait que l'océan global était complètement oxygéné au Néoprotérozoïque.

[Traduit par la Rédaction]

G.J. Baldwin, E.C. Turner, and B.S. Kamber.* Department of Earth Sciences, Laurentian Univeristy, 935 Ramsey Lake Rd, Sudbury, ON P3E 2C6.

Corresponding author: Geoffrey J. Baldwin (e-mail: gj_baldwin@laurentian.ca).

[1]Northwest Territories Geoscience Office Contribution 0052.
*Current address: Department of Geology, Trinity College Dublin, Dublin 2, Ireland.

Introduction

Neoproterozoic iron formations remain one of the most enigmatic rock types in the geologic record. Deposited during the last major pulse of Precambrian iron formation, these deposits have played a major role in the development of models for Earth's atmospheric and oceanic evolution. Neoproterozoic iron formations mark the reemergence of iron formation after roughly one billion years in which very few were deposited and have been interpreted to represent the termination of the controversial episode known as the "Canfield ocean". The observation that little to no iron formation was deposited during the Mesoproterozoic, with the exception of those in direct association with hydrothermal vent sites (e.g., Slack et al. 2007), paired with a shift to heavier sulphur isotopes, led some workers to suggest that the Mesoproterozoic deep ocean was euxinic (e.g., Canfield 1998; Farquhar et al. 2010) and that the reappearance of iron formation in the Neoproterozoic records the termination of that condition. In addition to the absence of iron formation during the Mesoproterozoic, the first series of redox condition studies of shale basins, using iron speciation (e.g., Shen et al. 2002, 2003; Poulton et al. 2004), and molybdenum isotopes (Arnold et al. 2004), argued in favour of a euxinic ocean, although each of these basins has been independently shown to have been restricted from the open ocean (e.g., Pufahl et al. 2010). Shales deposited in such basins are thus unlikely to record open-marine conditions. More recent studies that have good spatial and stratigraphic control both in the latest Paleoproterozoic (Poulton et al. 2010) and in the Neoproterozoic (Canfield et al. 2008; Johnston et al. 2010; Li et al. 2010) have shown that limited euxinia existed in shallow, coastal waters, whereas ferruginous conditions dominated deeper basins. This suggests that a true Canfield ocean, as originally defined, may never have existed and that the stratified water column more closely resembled the conditions reported in the more recent studies (Poulton and Canfield 2011). If the Mesoproterozoic ocean was not euxinic, the relative lack of iron formation during that time requires a new explanation. Kump and Seyfried (2005) suggested that there was a major change in the composition and flux of hydrothermal vent fluids, whereas Bekker et al. (2010) observed that the Mesoproterozoic was a time of relatively few mantle plume events. Neither of these explanations fully address why so little iron formation was deposited in an otherwise ferruginous ocean. Others have proposed that the deposition of Neoproterozoic iron formation was the result of a Neoproterozoic oxygenation event (NOE) that had significant influence on the chemical and biological development of the planet prior to the Cambrian explosion, including triggering a final pulse of iron formation deposition (Shields-Zhou and Och 2011).

The universal association of Neoproterozoic iron formation with glacial deposits attributed to the "snowball" Earth interval has led some workers to suggest that iron formation may have been closely associated with glacial episodes throughout the Precambrian (Young 1988, 2002), despite the lack of glacial deposits associated with most of the largest Paleoproterozoic iron formations. In this context, it is important to recall that the overwhelming majority of Neoproterozoic iron formations are associated with a single glaciation, the Sturtian glaciation (e.g., Hoffman and Li 2009; Macdonald et al.

2010b). A few iron deposits have poor age constraints and are believed to be of Marinoan age (e.g., Trompette et al. 1998; Kianian and Khakzad 2008). Only one is associated with the much later Ediacaran–Gaskiers glaciation (Pecoits et al. 2008). Another common attribute of the Neoproterozoic glaciogenic deposits, and therefore the iron formations themselves, is their close spatial link with rift basins that are associated with the initial breakup of Rodinia (Young 1992), which some have suggested were the direct cause of the glaciations (Young 2002; Eyles 2008). In summary, because of the conflicting views on the significance of geochronological and paleoenvironmental data for both the glacial events and iron formation deposition, the nature of the relationship between Neoproterozoic iron formation and glaciation remains largely unresolved.

A surprising concern is that in spite of the numerous outstanding questions that remain about the geodynamic, chemical, and oceanic constraints on Neoproterozoic iron formations, modified versions of the early depositional models for Neoproterozoic iron formation, such as that of Klein and Beukes (1993), continue to be applied to Archean iron formation (e.g., Beukes and Klein 1992). As a consequence, the geological implications of past studies of Neoproterozoic iron formation may far exceed the direct significance of the rocks themselves.

Specialized chemical and isotopic data extracted from Neoproterozoic iron formation are widely used in reconstructions of the Earth's surficial evolution, regardless of the fact that they are poorly understood compared with their older counterparts (e.g., Frei et al. 2009; Konhauser et al. 2009; Planavsky et al. 2010b). One of the core reasons for this lack of understanding is the relative paucity of comprehensive geochemical data for the Neoproterozic iron formations. Previous geochemical studies (e.g., Klein and Beukes 1993; Lottermoser and Ashley 2000; Klein and Ladeira 2004) were limited by the quality of the trace element data available. Because of the use of instrumental neutron activation analysis (INAA) in previous studies, only limited trace element data sets were obtained. The inability of this technique to measure many different trace elements, most notably the monoisotopic rare-earth elements (REE), has hitherto precluded an in-depth analysis of the marine chemistry controlling the deposition of the iron formation. With the advent of improved quadrupole inductively coupled plasma – mass spectrometry (ICP–MS) techniques that allow for the precise analysis of suites of more than 40 trace elements, including all of the REE, it is crucial to revisit the geochemistry of Neoproterozoic iron formations to properly understand the geochemical and oceanographic conditions that influenced their deposition.

This study addresses the Rapitan iron formation, one of the most prominent and archetypical Neoproterozoic iron formations, using the REE, with the addition of yttrium, to assess the general chemical nature of the basin. The redox evolution and configuration of the basin are interpreted using recent advances in understanding the behaviour of redox-sensitive trace metals, such as Mo and U, in modern basins. A proper understanding of the Rapitan iron formation's depositional basin, as well as those of other Neoproterozoic iron formations, is critical to using these deposits to model the evolution of Earth-surface environments.

Geological setting

The Rapitan Group (lower Windermere Supergroup) is exposed in the northern Canadian Cordillera, in the Northwest Territories and Yukon (Fig. 1). In the Mackenzie Mountains, the Windermere Supergroup consists of the basal Coates Lake Group, the Rapitan Group, the Hay Creek Group (Yeo 1978; James et al. 2001), and several ungrouped late Neoproterozoic formations (Aitken 1989; Narbonne and Aitken 1995; Fig. 2). In Yukon, the Coates Lake Group is absent, and the Rapitan Group lies directly on strata of the early Neoproterozoic Mackenzie Mountains supergroup. This thick (~4–5 km) succession consists of shallow-marine carbonate rocks, fluvial quartz arenite, marine siltstone and minor shale, and evaporite rocks (Long et al. 2008).

The Rapitan Group is underlain by the Coates Lake Group in the Redstone River – Mountain River region of the Mackenzie Mountains and by the Little Dal Group in the Snake River region of the Northwest Territories and Yukon (Yeo 1981) (Fig. 2). Both the Coates Lake and Rapitan groups were deposited in extensional settings associated with the initial rifting of the supercontinent Rodinia (Young 1992), and there is local evidence for a slight angular unconformity between the two groups, as well as within the Rapitan Group (Helmstaedt et al. 1979). The sedimentological evidence of pronounced lateral thickness and lithofacies, combined with the observed angular unconformities, indicate that these groups were deposited on an actively rifting margin, which would have generated fault grabens, promoted basin restriction, and possibly caused glaciation (Eyles 2008; Young 2002). The Coates Lake Group consists of the "Little Dal basalt", the Thundercloud, Redstone River, and Coppercap formations; sedimentary-hosted copper deposits are associated with the Redstone River – Coppercap contact (e.g., Rose et al. 1986; Jefferson and Ruelle 1987; Jefferson and Parrish 1989; Narbonne and Aitken 1995). The stratigraphic affiliation of the Coates Lake Group has been the subject of dispute: some authors suggest that it belongs to neither the Mackenzie Mountains supergroup nor the Windermere Supergroup (Jefferson and Parrish 1989). The current consensus, however, is that it represents the basal Windermere Supergroup (e.g., Narbonne and Aitken 1995; Long et al. 2008). Overlying the Rapitan Group in the Redstone River region (Fig. 1A) is the Hay Creek Group (Yeo 1978; James et al. 2001), the lowermost formation of which is the Twitya Formation, which contains disc-shaped impressions that are purported to be the oldest documented physical evidence of metazoans (Hofmann et al. 1990). The Hay Creek Group is conformably overlain by several ungrouped formations of the upper Windermere Supergroup, which extends through to the lower Cambrian (Aitken 1989). In the Snake River region (Fig. 1B), the Rapitan Group is unconformably overlain by the lower Paleozoic Franklin Mountain and Mount Kindle formations.

The Rapitan Group was established by Green and Godwin (1963) for a succession of diamictite and iron formation, although the presence of iron formation in the Snake River region had been known as early as the Yukon gold rush (Keele 1906) and was identified elsewhere in the Mackenzie Mountains soon after (Keele 1910). Siliciclastic rocks associated with the iron formation were first interpreted to be of

glaciogenic origin by Ziegler (1959), a conclusion that was later confirmed by other authors (e.g., Eisbacher 1976, 1978, 1981a, 1981b, 1985; Young 1976; Yeo 1981). The stratigraphy of the Rapitan Group was studied extensively by Eisbacher (1978), who established type sections for the Sayunei and Shezal formations in the Redstone River region. The Sayunei Formation consists of dark red to maroon, deepwater, fine-grained turbidites, locally capped by thin jaspilitic iron formation in the Redstone River area, and is overlain by green, grey, or tan diamictite of the Shezal Formation (Eisbacher 1978; Yeo 1981). In the Snake River region, the iron formation is significantly thicker (up to 120 m) and was the target of extensive exploration for iron ore in the 1960s (Stuart 1963). The stratigraphic position of the iron formation in this region is the subject of some dispute. Klein and Beukes (1993) contend that it is at the top of the Sayunei Formation, as is the case to the southeast in the Redstone Plateau area, whereas Yeo (1981) placed it in the lowermost Shezal Formation. Diamictite of the areally limited Mount Berg Formation underlies the Sayunei Formation only in the southernmost part of the Rapitan exposure area (Eisbacher 1978; Yeo 1981).

A granitic dropstone from the lower Sayunei Formation yielded a U–Pb zircon age of 755 ± 18 Ma, providing a maximum depositional age for the Rapitan Group (Ross and Villeneuve 1997). Macdonald et al. (2010a) obtained a U–Pb zircon age of 716.47 ± 0.24 Ma from a felsic tuff interbedded with the possibly equivalent upper Mount Harper Group of the central Ogilvie Mountains, western Yukon (Yeo 1981), which was interpreted to imply that volcanism and iron formation were coeval within the larger basinal context. These ages are consistent with the estimated age of the Sturtian glaciation, the oldest of the major glacial episodes associated with the "snowball" Earth hypothesis (e.g., Kirschvink 1992; Hoffman et al. 1998). The Sturtian affiliation of the Rapitan Group is indirectly supported by the presence of another Neoproterozoic glaciogenic unit higher in the Windermere Supergroup, the Ice Brook Formation, which is attributed to the Marinoan glacial event (Aitken 1991a, 1991b; James et al. 2001).

Stratigraphy

A detailed stratigraphic section of the Rapitan iron formation was measured near the Cranswick River, Northwest Territories (Fig. 3). This easternmost exposure of the Snake River deposit of the Rapitan iron formation (65°12.856′N and 132°22.105′W) contains ~30 m of hematite–jasper iron formation. Most of this deposit (called the Crest or Snake River deposit) is located in Yukon. Good exposure in the Northwest Territories is limited to a series of incised canyons along the mountainsides east of the Cranswick River, one of which contains a complete exposure of the iron formation, as well as variable exposure of the underlying and overlying clastic, glaciogenic rocks.

Attempts to use the iron-formation textural classification scheme of Beukes and Gutzmer (2008) proved ineffective. Rapitan iron formation lithofacies are best referred to as hematite–jasper felutite (N.J. Beukes, personal communication, 2010). Here, however, a Rapitan-specific classification scheme is used. The iron formation rocks are generally either

Fig. 1. Geological map of the approximate distribution of Proterozoic strata of northwestern Canada and eastern Alaska. Inset map shows the location of the geological map. The Rapitan Group and its equivalents in the Oglivie Mountains (western Yukon and eastern Alaska) are in red (in online version). The Redstone River region (A) and the Snake River region (B) are indicated (modified from Yeo 1981).
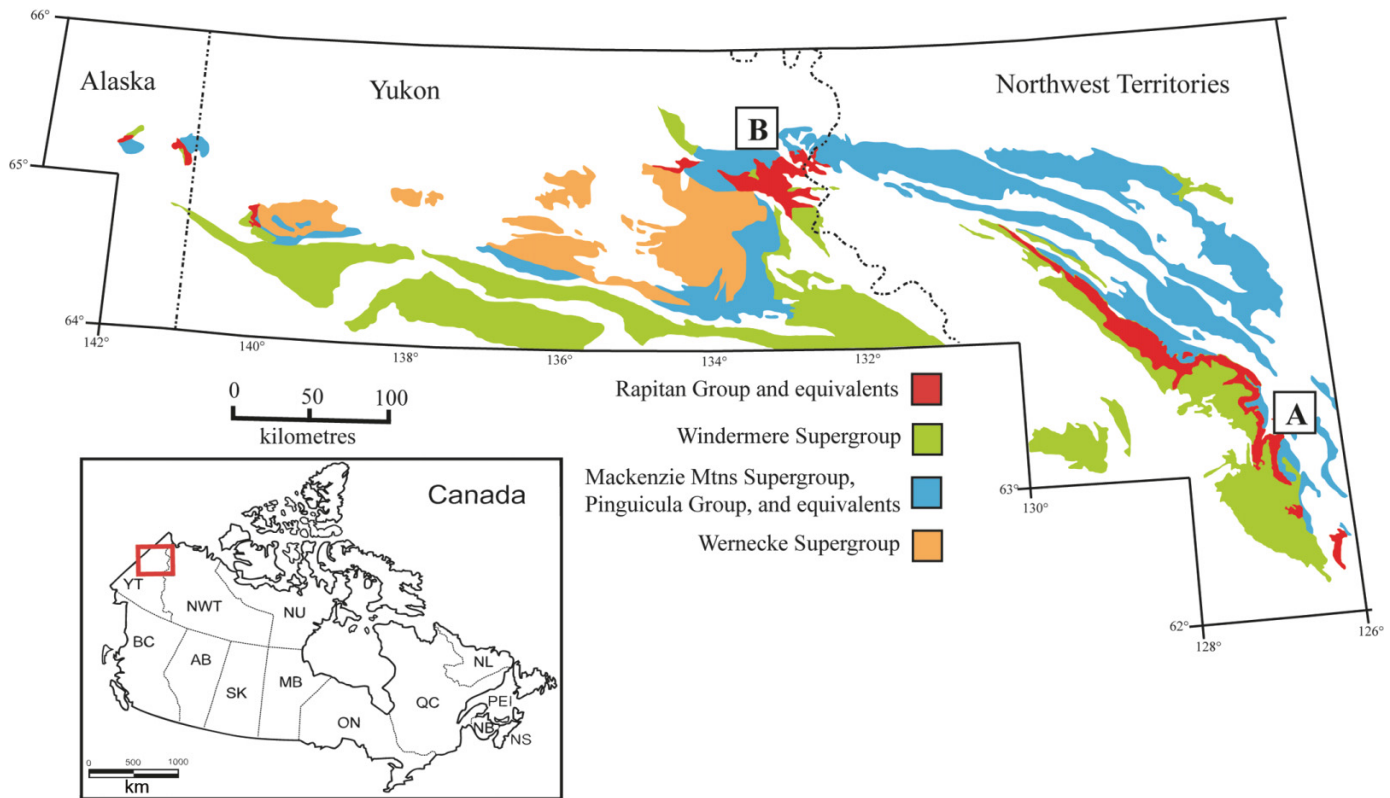
layered jasper and hematite (i.e., banded iron formation (BIF)) or nodular iron formation, which consists of massive hematite and subspherical to elongate, zoned jasper nodules (Figs. 4A, 4B). The most elongate of the nodules have been referred to as "lenticles" (Yeo 1981) or lenses, can be up to a metre in lateral extent, and may be of either syndepositional or very early diagenetic origin (Fig. 4C). These two types of iron formation are end members, and most units are transitional between the two; each unit is classified according to whether beds or nodules are the dominant form of jasper. The term "jasper" is quite useful for these rocks because Rapitan cherts exhibit a considerable range in iron content, and vary in colour from yellow–orange to purple.

The iron formation is underlain by a polymictic, clast-supported, channel-fill conglomerate containing predominantly carbonate and quartz arenite clasts derived from the underlying Mackenzie Mountains supergroup, as well as scattered basaltic clasts of uncertain provenance. Clasts are pebble- to cobble-grade, and rare boulders are present. The intergranular space contains carbonate cement and scattered quartz sand grains. The conglomerate has variable lateral thickness and continuity and is hosted in a friable, clast-rich, purple intermediate diamictite with clast lithologies that are similar to those of the conglomerate. The contact between the conglomerate–diamictite and the iron formation is in a thin covered interval, above which is a 2 m thick succession of siltstone and sandy siltstone. These clastic layers are hematite-cemented and contain scattered dropstones, predominantly of carbonate composition, weak normal grading, and faint cross-bedding. Similar units recur

throughout the iron formation but are rarely more than a few tens of centimetres thick.

Above the basal clastic interval, the iron formation consists of variably interbedded BIF and nodular iron formation units. Continuous jasper beds are common in nodular units, particularly in the thicker intervals of this rock type. Ubiquitous dropstones are typically of carbonate composition, and generally deform only 1–2 cm of underlying iron formation, if any (Fig. 4D). Some iron formation (IF) intervals are very dropstone-rich, containing more than 70% dropstones of mixed composition (mostly carbonate) in a predominantly hematitic matrix, with dropstone grain sizes ranging from granules to large pebbles (this lithofacies is here referred to as "dropstone-rich IF"). The iron formation contains irregular bedding in some intervals and local slump folds. Slump folds are most conspicuous in the vicinity of a large slump scar that is between 5 and 10 m above the base of the iron formation. The surface crosscuts up to 3 m of strata and is associated with considerable reworking and folding in its lateral equivalents. A few intervals in the main measured section are extensively reworked, such that they no longer resemble typical iron formation, and the primary relationships between the folded and disjointed jasper beds, hematite beds, and jasper nodules are not clearly discernible; these units are referred to as "slumped or reworked IF".

The relative ratio of BIF to nodular iron formation increases in the uppermost 15 m of the iron formation, although nodular iron formation remains abundant, as do nodular layers in the BIF. Unlike the lower part of the section, the upper part of the iron formation contains jasper nod-

Fig. 2. Generalized Neoproterozoic stratigraphy of the Mackenzie Mountains, Northwest Territories, and Yukon, showing the stratigraphic position of the Rapitan Group in the Windermere Supergroup and its position relative to the older Mackenzie Mountains supergroup and the Neoproterozoic–Cambrian boundary. H1 is the informal stratigraphic name for the basal unit of the Mackenzie Mountains supergroup.
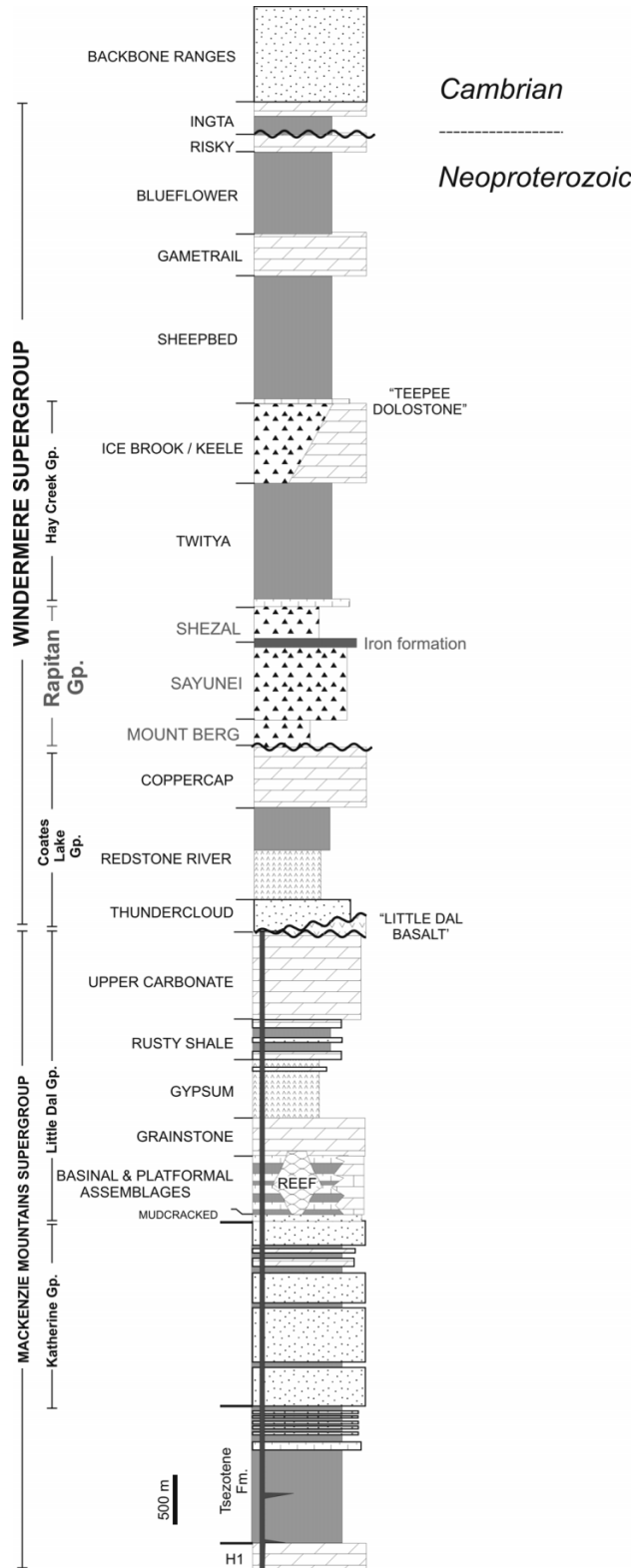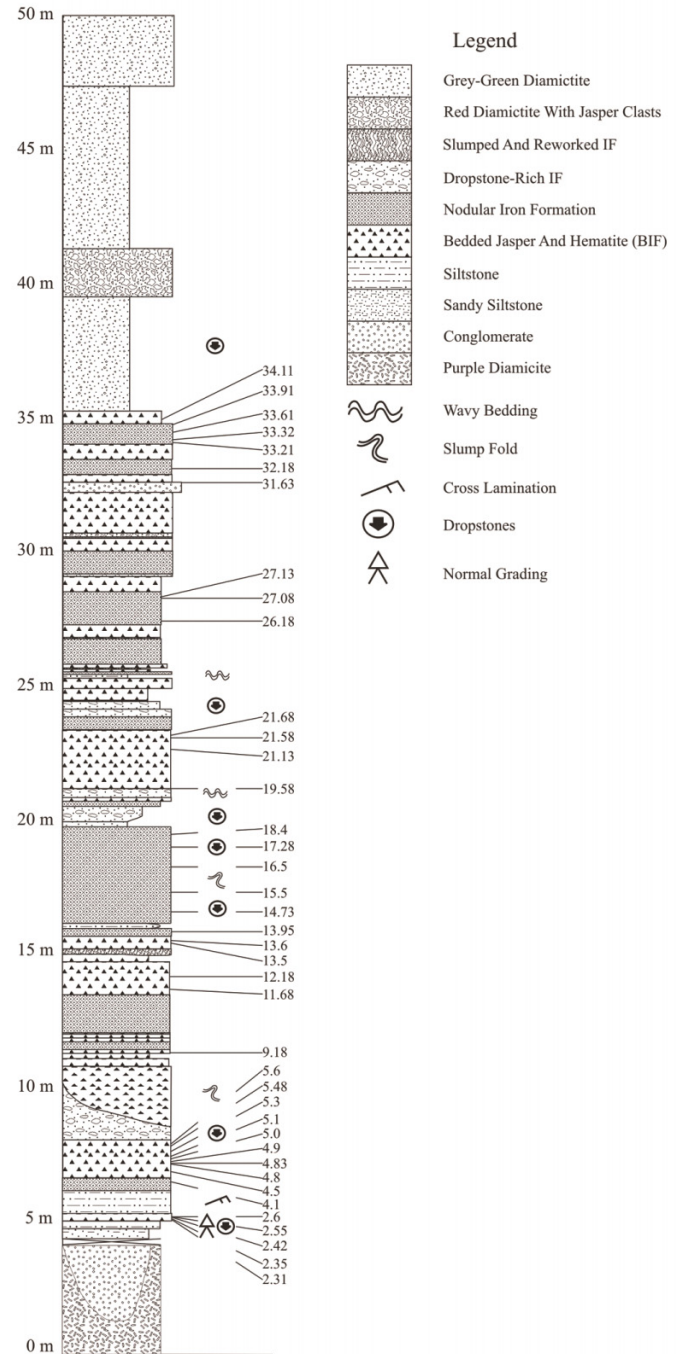

Fig. 3. Stratigraphic column of the Rapitan iron formation at Cranswick River, Northwest Territories. Sample numbers that correspond with stratigraphic position are located on the right side of the column. Lithofacies listed in the legend correspond to those referred to in the text. IF, iron formation; BIF, banded iron formation.

ules in jasper beds; these nodules are generally not zoned, and commonly have a fairly subtle colour difference from the host jasper. Consequently, although these units are referred to as bedded jasper, or BIF units, a strong case can be made for their classification as nodular iron formation because a far greater proportion of the jasper is in the nodules than in the bands (Fig. 4E). The uppermost jasper bed, at the contact between the iron formation and overlying diamictite,

Fig. 4. (A) Typical bedded jasper and hematite banded iron formation that was the primary sampling target. (B) Zoned jasper nodules are ubiquitous in the Rapitan iron formation, here in a matrix of massive hematite. (C) Elongate, lenticular nodules, or "lenticles", in a thick package of hematite and nodules, with very few true jasper bands. (D) Dropstones, of predominantly resedimented carbonate clasts, deform only a maximum of a few millimetres of underlying sediment. (E) Jasper nodules can also be hosted in jasper bands, a potential hazard when sampling for geochemical analysis. (F) Grey–green chert nodules are present only in the uppermost jasper band of the iron formation.
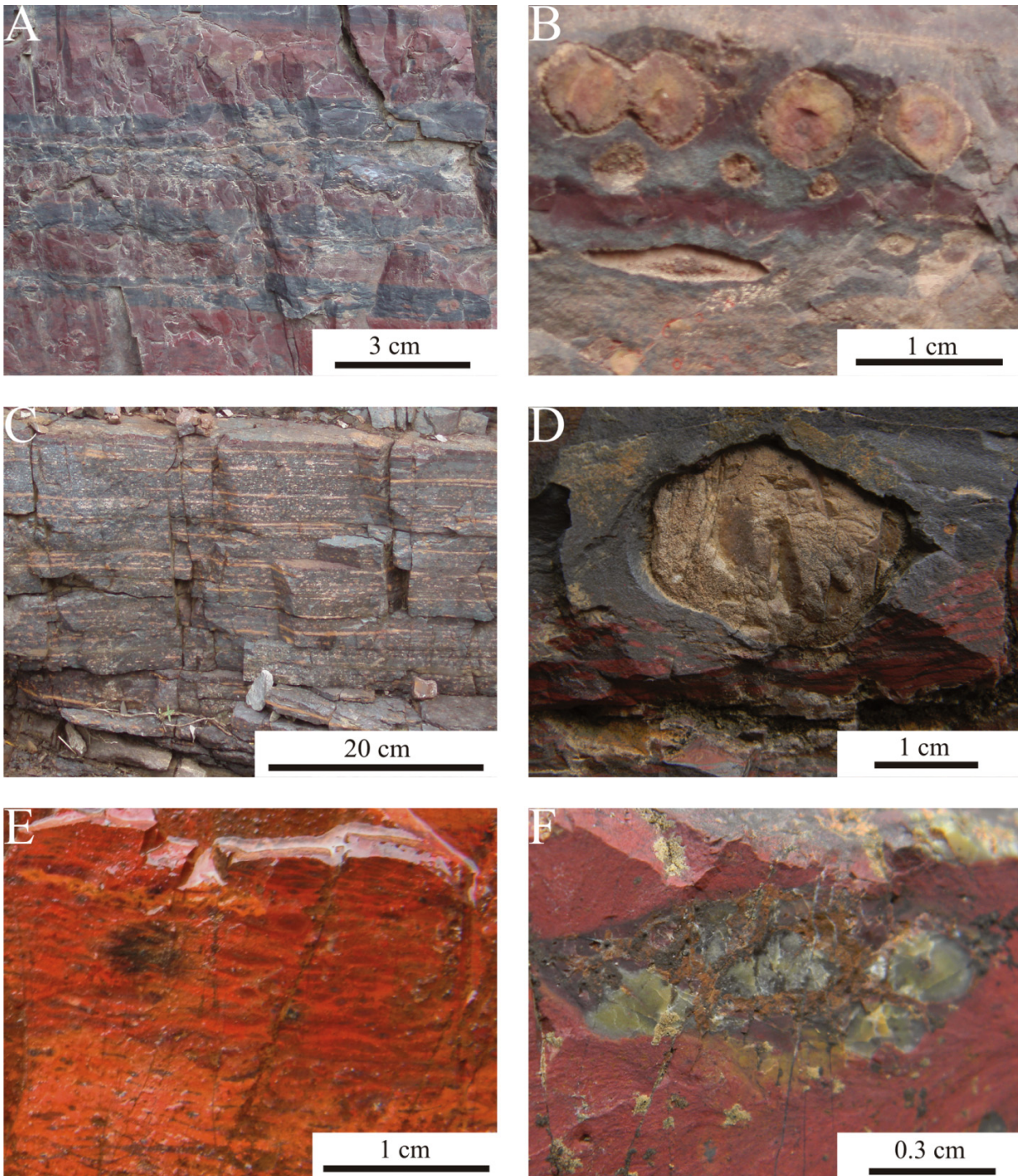
contains greenish tan chert nodules in a jasper matrix; this is the only non-jaspilitic chert in the section (Fig. 4F).

Overlying the iron formation are at least 15 m of texturally and compositionally variable diamictite. These are dominated by grey–green to tan, carbonate-rich, sandy clast-rich pebble diamictite, commonly with a fissile, scaly weathering style that is typical of Shezal Formation diamictite. The exception to this is a roughly 2 m thick unit of well-indurated red diamictite containing abundant jasper clasts, many of which show evidence of resedimentation prior to lithification. Some elongate clasts are vertically oriented, which may be evidence of either rapid sedimentation or reworking of locally derived

iron formation. Based on the sedimentological evidence offered by the siliciclastic rocks that underlie and overlie the iron formation at this site, the stratigraphic position of the iron formation is entirely within the Shezal Formation, as per Yeo (1981), but further work is needed in the area to confirm this.

Methods

Forty-two jasper samples were analysed for major and trace element geochemistry. Following the procedures outlined by Baldwin et al. (2011) and Ulrich et al. (2009), exploratory laser-ablation – inductively coupled plasma – mass spectrometry (LA–ICP–MS) analyses were performed on both jasper bands and nodules to screen for homogeneity. Jasper bands are highly homogeneous, whereas the nodules exhibit both concentric and discordant chemical zoning, and were therefore considered less suitable for the purpose of this study. Furthermore, because the nodules are undoubtedly of an early diagenetic origin, they probably do not record true basinal seawater conditions. It has been suggested that chert beds in iron formations containing ferrous iron species, such as siderite and magnetite, could also be diagenetic in origin (Fischer and Knoll 2009), but this idea has not been extended to hematite–jasper iron formations.

Trace elements were analysed by quadrupole ICP–MS at Laurentian University, Sudbury, Ontario, following the digestion methods of Babechuk et al. (2010) and Baldwin et al. (2011), and a mass spectrometric approach similar to that of Eggins et al. (1997), using modifications reported in Kamber (2009) and Babechuk et al. (2010). Element concentrations were externally calibrated using multiple solutions of the United States Geological Survey (USGS) standard W-2. The international rock standards JA-2, JB-2, and IF-G were analysed as unknowns and compared with the laboratory long-term reproducibility (e.g., Kamber 2009). Weight percent major element oxides were measured using X-ray fluorescence (XRF) at the Ontario GeoLabs, Sudbury, Ontario, for 20 samples, and by ICP–MS for the remaining 22 samples at Laurentian University. Samples measured by ICP–MS lack data for SiO_2 and loss on ignition (LOI) because of the digestion methods used. More detail about methods, full data tables, and related figures are available in supplementary materials.[2]

Results

Rare-earth elements and yttrium (REE+Y) systematics

There is a surprising lack of modern high-quality chemical data, especially the REE+Y, for Neoproterozoic chemical sediments (including iron formation), which contrasts with a rich literature on comparable Archean and Paleopoterozoic materials. This is unfortunate because the behaviour of the REE+Y in modern seawater is well understood. Depletion of the light rare-earth elements (LREE) relative to the heavy rare-earth elements (HREE), superchondritic Y/Ho ratios, and positive anomalies of both La and Gd are all characteristic of modern seawater (e.g., Zhang and Nozaki 1996), and have been reported for hydrogenous sediments from the entire geological record (e.g., Bau and Dulski 1996; Nothdurft

et al. 2004; Alexander et al. 2008; Planavsky et al. 2010*a*), which points to the extreme antiquity of the hydrological cycle (Kamber 2010). Although some authors have contended that the REE composition of seawater has changed significantly over time (e.g., Picard et al. 2002), others point out that these reported changes in the marine REE budget are an artefact of using marine phosphates as a seawater proxy, which inherently fractionates the REE from ambient seawater compositions (Shields and Webb 2004). There is little doubt that changes in the overall slope of the normalized REE pattern and the size of the Y, La, and Gd anomalies may have changed over time (Kamber 2010), but the only substantial temporal deviations exist for the redox-sensitive Ce and Eu (as explained later in the text). The remarkable similarity of the REE patterns in modern seawater and normal marine hydrogenous rocks from throughout time (Fig. 5C) is interpreted to reflect the extreme antiquity of the marine REE cycle. The diagnostic features of the marine REE pattern have been demonstrated to be generated during the introduction of dissolved REE+Y from riverine sources into the ocean. In an estuary, LREE are more readily removed by adhesion to organometallic complexes than are the HREE, Y, La, and Gd (Elderfield et al. 1990; Lawrence and Kamber 2006). It is noteworthy that seawater-type REE patterns can form in saline aquifers (Johannesson et al. 2006), but such a setting clearly does not apply to sediment of proven marine origin. In addition to these features, europium (Eu) and cerium (Ce) are critical tools for understanding Precambrian seawater because they deviate from normal trivalent REE behaviour. Europium can be used as a proxy for the contribution of hydrothermal fluids to ocean water because of the large positive Eu anomalies of modern high-temperature hydrothermal fluids (e.g., Bau and Dulski 1999). The presence of positive Eu anomalies even in shallow-water Paleoproterozoic iron formation and microbial carbonate strongly suggests long-distance transport of Eu^{2+} through an anoxic ocean (e.g., Derry and Jacobsen 1990). Because of differences in particle adhesion between Ce^{3+} and the oxidized ion Ce^{4+}, the Ce anomaly is a common proxy for oceanic paleoredox conditions. This behaviour typically results in negative Ce anomalies in oxidized seawater, but excess Ce in anoxic water below a chemocline (e.g., Ohta et al. 1999; Kato et al. 2006; Planavsky et al. 2010*a*). In summary, proper assessment of REE+Y systematics is an important starting point when examining any hydrogenous sedimentary rock.

In this study, REE+Y data were normalized to upper continental crust using the modern alluvial sediment average MuQ (Mud from Queensland, Australia, Kamber et al. 2005), which was produced with the same analytical protocol as the present study. Normalized data were initially screened for patterns demonstrating the two most diagnostic features of seawater REE+Y patterns: LREE depletion and a superchondritic Y/Ho ratio (Y/Ho > 26). Most of the data set (n = 33) exhibits these characteristics, but nine samples deviated from typical marine patterns (Figs. 5A, 4B). Of these nine samples, seven produced REE+Y patterns that were distinct from typical seawater in their overall shape or slope, and two demonstrated significantly greater LREE depletion than


Fig. 5. Shale-normalized rare-earth element and yttrium (REE+Y) diagrams of jasper samples from the Rapitan iron formation. (A) Most of the samples (*n* = 34) demonstrate fairly uniform, consistent, seawater-type patterns with pronounced positive slopes, small negative to flat Ce anomalies, positive Gd anomalies, and superchondritic Y/Ho ratios. (B) Nine other samples show nonseawater-type REE+Y patterns, commonly with unusual patterns that have not been interpreted, and have accordingly been eliminated from further discussion. These nine samples are identified in Table S2.[2] (C) Compilation of REE+Y data for seawater and hydrogenous sedimentary rocks through time. Modern shallow, median, and deep seawater compiled by Kamber (2010), showing deep negative Ce anomalies and positive La, Gd, and Y anomalies. Modern (Webb and Kamber 2000) and Devonian (Nothdurft et al. 2004) microbial carbonates show positive La and Y anomalies, with small negative Ce anomalies. Eoarchean (Bolhar et al. 2004) and Neoarchean (Baldwin et al. 2011) iron formation also show positive La, Gd, and Y anomalies, but without statistically significant Ce anomalies, and with pronounced positive Eu anomalies, showing that these (Ce/Ce* and Eu/Eu*, see Lawrence et al. 2006 for formula) are the only attributes of the REE+Y systematics of seawater that have changed significantly over Earth history. Comparison of the patterns in (A) with those in (C) demonstrates that they record the REE+Y composition of seawater that has remained largely unchanged throughout Earth history, and are thus the most appropriate samples to include in a study of the basinal seawater chemistry of the Rapitan iron formation. UCC, upper continental crust.

is expected for seawater: in the latter two samples, the HREE were enriched by more than two orders of magnitude relative to the LREE, whereas the HREE are typically enriched by approximately one order of magnitude in the rest of the data set (Fig. 5B). A basic assessment of other diagnostic trace element concentrations, such as Th, showed that these two samples were strongly influenced by a nonhydrogenous source and so do not reflect seawater chemistry, despite some similarities.

The patterns that do not reflect pure, hydrogenous chert (see Fig. 5C for examples) have limited use for reconstructing basin water chemistry. The nine samples may be influenced either by elevated phosphate mineral contents, which can cause nontrivalent fractionation of the otherwise nonanomalous REE, by detrital material whose trace element budget overwhelms the chert, or by late, low-temperature hydrothermal veins (primarily calcite). In view of the relative uniformity of all of the other patterns, no further effort was made to understand the nine incongruent patterns, and these samples are excluded from further discussion.

Cerium can be an interesting and direct window into the paleoredox conditions of the depositional basin in which a chemocline existed and in which particle transport involved Mn oxyhydroxides. Much like other REE studies of Neoproterozoic iron formation (e.g., Klein and Beukes 1993; Lottermoser and Ashley 2000; Klein and Ladeira 2004; Kato et al. 2006), the new data show that the Rapitan iron formation displays only limited variability in Ce/Ce* (see Lawrence et al. 2006 for formula), with values ranging from 0.8 to 1.07 for 33 samples, 19 of which fall between 0.95 and 1.05, indicating the absence of a significant Ce anomaly. Of the remaining 14 samples, seven fall between 0.8 and 0.95, and seven
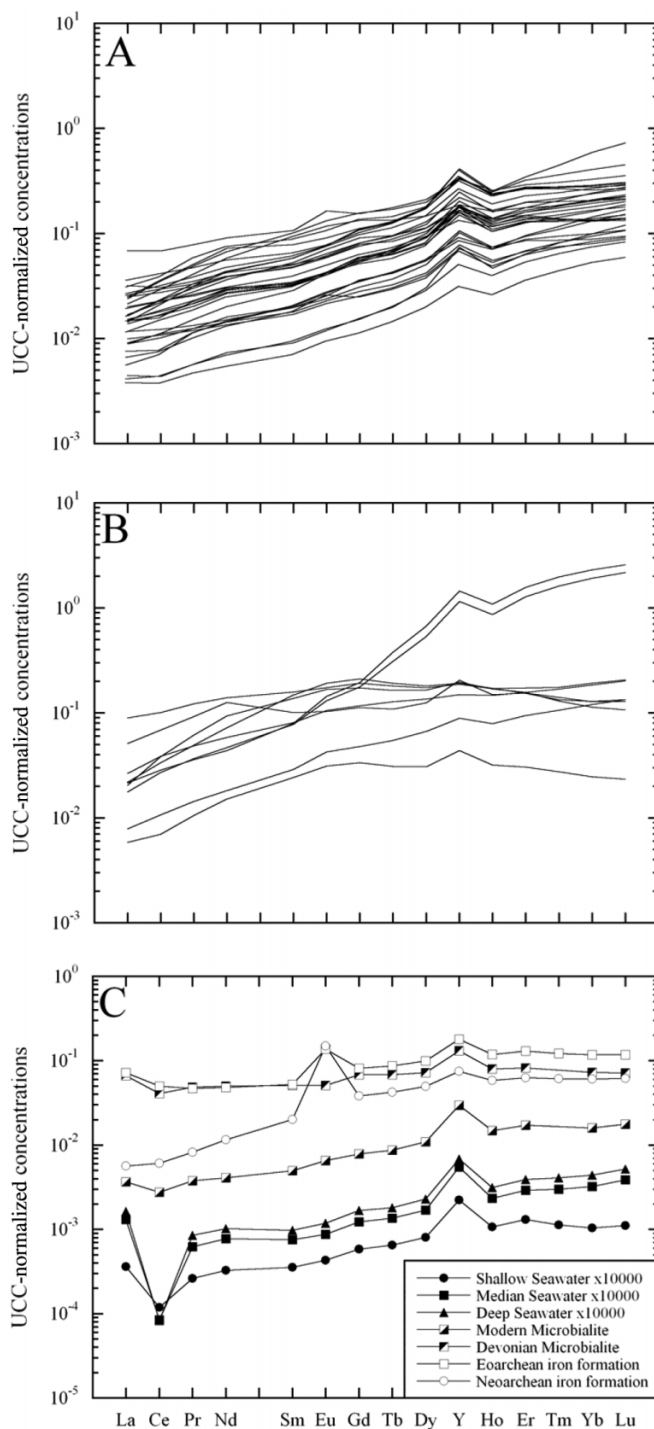
are between 1.05 and 1.07, demonstrating that the majority of the data set (*n* = 26) has either no statisically significant Ce anomaly or a very small negative anomaly. This suggests that seawater conditions were anoxic to very weakly oxic with respect to Ce. It is also critical to note the absence of a positive Ce anomaly. Planavsky et al. (2010*a*) demonstrated a tendency for some late Paleoproterozoic iron formations (e.g., Gunflint iron formation) to produce flat to positive Ce anomalies. They interpreted this tendency to reflect a Mn-particle shuttle across a redoxcline. Below such a redoxcline, Mn particles dissolve and Ce^{4+}, which was preferentially scavenged relative to the trivalent REE from the oxidized

upper water column, was released, thereby producing an overabundance of Ce below the redoxcline. This can result in pronounced positive Ce anomalies in BIF deposited in such settings. The absence of any meaningful positive Ce anomaly in the new Rapitan data suggests that any particulate shuttle in the Rapitan Basin was not dominated by Mn oxides and was probably defined by an iron shuttle and redoxcline, similar to that suggested for Archean and early Paleoproterozoic iron formations (Planavsky et al. 2010a).

Despite its origin from high-temperature hydrothermal vent fluids, a Eu anomaly is common in most Archean and Paleoproterozoic hydrogenous sediments, including iron formation and shallow-water microbial carbonate. This characteristic has led to oceanic circulation models that involve a sufficiently anoxic ocean to allow for the long-distance transport of Eu^{2+}, and therefore Fe^{2+}, from its most important source, vent systems along midocean ridges (Derry and Jacobsen 1990; Isley 1995). An alternative explanation is the proposed relationship of iron formation deposition and mantle plume events (e.g., Isley and Abbott 1999; Bekker et al. 2010); unusually large volumes of hydrothermally sourced Eu and Fe are postulated to have been released into the ocean during such events. The lack of a positive Eu anomaly in the majority of samples studied here is clearly inconsistent with these models for iron formation genesis and with the source of the iron. Only two samples have Eu/Eu* (see Lawrence et al. 2006 for formula) values above 1.1, whereas the bulk of the data set ($n = 25$) has Eu/Eu* values of 1.0 or less. This consistent lack of a Eu anomaly is significant and imposes strong constraints on depositional models. In brief, the simplest explanation for the missing Eu anomaly is that the open ocean was sufficiently oxygenated in the Neoproterozoic that long-distance transport of Eu was inhibited through co-precipitation with Fe-oxide phases (Bau and Dulski 1999). The only plausible alternative explanation is that the basin was almost completely isolated from the open ocean, meaning that its sediment would be inappropriate for reconstructing global oceanic conditions, or inferring a global sheet of sea ice. Both of these explanations are incompatible with a hydrothermal iron source for the Rapitan iron formation because hydrothermal Fe^{2+} and the positive Eu anomaly are cogenetic features in iron formation.

The new Rapitan data express three of the most common and meaningful REE+Y features: HREE-enrichment, a positive Gd anomaly, and a Y anomaly (expressed as Y/Ho). Heavy rare-earth element enrichment, indicated by a positive overall slope in the REE+Y pattern, is best calculated as the Pr_{SN}/Yb_{SN} ratio because these are the lightest and heaviest elements that behave in a manner that is strictly determined by ionic radius (La, Ce, and possibly Lu behave differently in marine systems). Hydrogenous sediment precipitated from normal seawater should demonstrate very low Pr_{SN}/Yb_{SN} ratios because Yb should have a much greater normalized abundance than Pr. The samples studied here show a fairly tight range of very low Pr_{SN}/Yb_{SN} ratios (~0.05–0.2), indicating strong enrichment of the HREE relative to the LREE. Similarly, superchondritic Y/Ho ratios are a ubiquitous feature in such rocks, with any values greater than Y/Ho = 26 considered indicative of quantifiable hydrogenous influence on a detrital REE pattern. The new data show a fairly wide range of superchondritic values, ranging from 29.9 to 42.5,

Fig. 6. (A) Y/Ho ratios plotted against the Gd anomaly (Gd/Gd*, see Lawrence et al. 2006 for formula). Y/Ho and Gd/Gd* are strongly correlated, with $r^2 = 0.71$. (B) Y/Ho ratios plotted against Al_2O_3 concentrations (wt.%). Al_2O_3 does not have a relationship with the Y/Ho ratio, with the full range of Y/Ho values occurring at near-constant Al_2O_3 concentrations. Samples with elevated Al_2O_3 show a wide range of Y/Ho ratios, indicating that detrital input exerted minimal control on the Y/Ho ratio. The variability in Y/Ho and the Gd anomaly, therefore, reflects the existence of distinctive water chemistries in the basin and not detritally controlled variability.
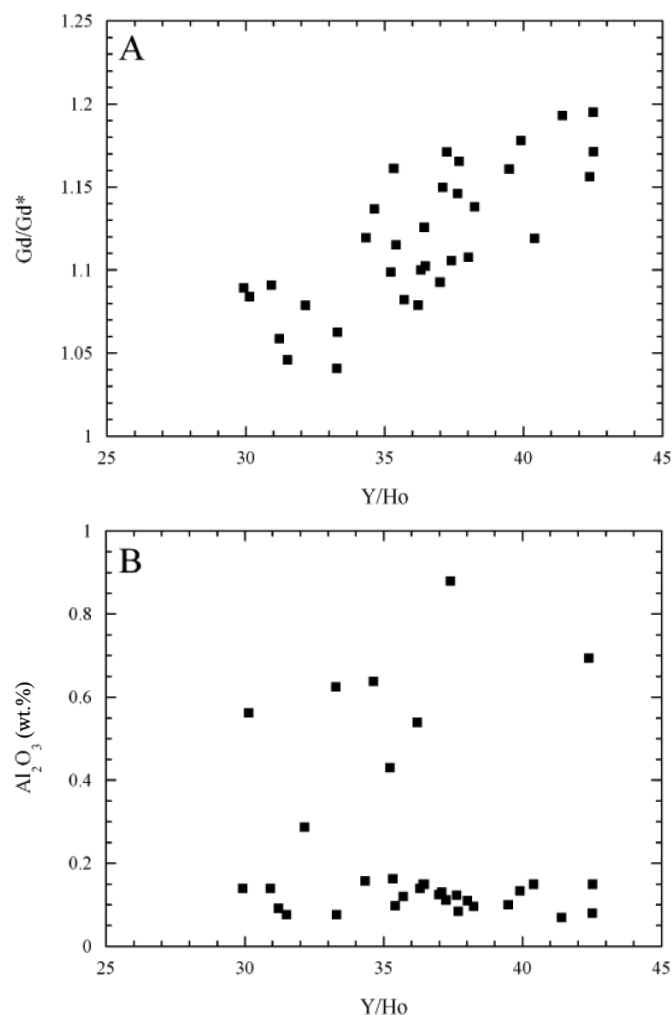

as well as relatively variable but consistently positive Gd anomalies (Gd/Gd* = 1.04–1.19, see Lawrence et al. 2006 for formula). All three of these features (low Pr_{SN}/Yb_{SN} ratios, superchondritic Y/Ho ratios, and positive Gd anomalies) are hallmarks of normal marine seawater, and despite their individual variability, suggest that the Rapitan Basin must have been connected to the open ocean, an assertion further reinforced by the reasonably strong positive correlation between the Y/Ho ratio and the Gd/Gd* values ($r^2 = 0.72$; Fig. 6A). The rather large but strongly correlated range of these values, particularly the Y/Ho ratio, points to some variability either in the degree of clastic contamination or in the basin water chemistry. The most common mechanism for causing such ranges is dilution of the seawater signature by detrital material such as clay minerals (e.g., Baldwin et al.

Fig. 7. The Eu anomaly (Eu/Eu*, see Lawrence et al. 2006 for formula) plotted against (A) Y/Ho, (B) Gd/Gd* (see Lawrence et al. 2006 for formula), and (C) Al_2O_3. No statistically significant correlation is found between the Eu anomaly and either Y/Ho or Gd/Gd*. Dotted lines indicate Eu/Eu* = 1, or the threshold for the Eu anomaly. This indicates that positive Eu anomalies are not of open-marine origin and that the wider ocean did not carry a positive Eu anomaly. Samples with Eu/Eu* values greater than the statistically significant 1.1 also contain elevated Al_2O_3 concentrations relative to the majority of the data set. This suggests that the positive Eu anomalies can be attributed to input of older detritus with positive Eu anomalies (e.g., feldspar) into the iron formation, rather than from a contemporaneous hydrothermal source, as noted by Klein and Beukes (1993).


2011). The flat shale-normalized REE patterns of clays, and their much higher overall REE concentrations (relative to hydrogenous sediments), combine to dilute recorded seawater anomalies, such as Y/Ho ratios, even with as little as 1%–2% by weight clastic contamination. This can be easily addressed, however, by plotting the Y/Ho ratios against the concentration of an immobile lithophile element, such as Al (Fig. 6B). The complete lack of a relationship between the Y/Ho ratio and Al, as well as several other immobile elements (e.g., Ti, Th, Ga) indicates that the documented variability in the Y/Ho ratio is not a function of the amount of detrital input. The variation was, therefore, probably the result of variable water chemistry (over the duration of the Rapitan deposition) caused by moderate but variable degrees of basin restriction, in which the basin had sufficient connectivity with the open ocean to maintain a strong correlation between Y/Ho and Gd/Gd*, while simultaneously being restricted enough to allow for considerable variability in the same values.

Neither the Y/Ho ratio nor the Gd anomaly correlates clearly with the Eu anomaly (Figs. 7A, 7B). Instead, there are two weakly developed trends of inverse correlation, but no well-defined trend exists for the entire data set. The few samples that have more elevated Eu anomalies show smaller Gd anomalies and relatively low Y/Ho ratios, indicating that the few positive Eu anomalies present are not of an open-marine origin. Furthermore, the samples with the largest positive Eu anomalies contain elevated concentrations of Al relative to the bulk of the data set (Fig. 7C). This suggests that the largest positive Eu anomalies resulted from the input of older detrital material that was overenriched in Eu (e.g., feldspar), which is consistent with the observations of Klein and Beukes (1993) that positive Eu anomalies were only present in samples containing volcaniclastic detritus. Naturally, not all samples with elevated Al also demonstrated positive Eu anomalies because not all of the detrital material supplied would have been from Eu-rich phases, and indeed the samples with the highest Al have Eu/Eu* values that are consistent with the majority of the sample suite, indicating that most detrital input was from Eu-poor clay minerals. Therefore, regardless of whether an open-marine signal was modified in the Rapitan Basin by a more local water mass, the lack of positive Eu anomalies in the samples with the highest Y/Ho and strongest positive Gd anomalies constitutes firm evidence that the Neoproterozoic ocean no longer had a positive Eu anomaly.
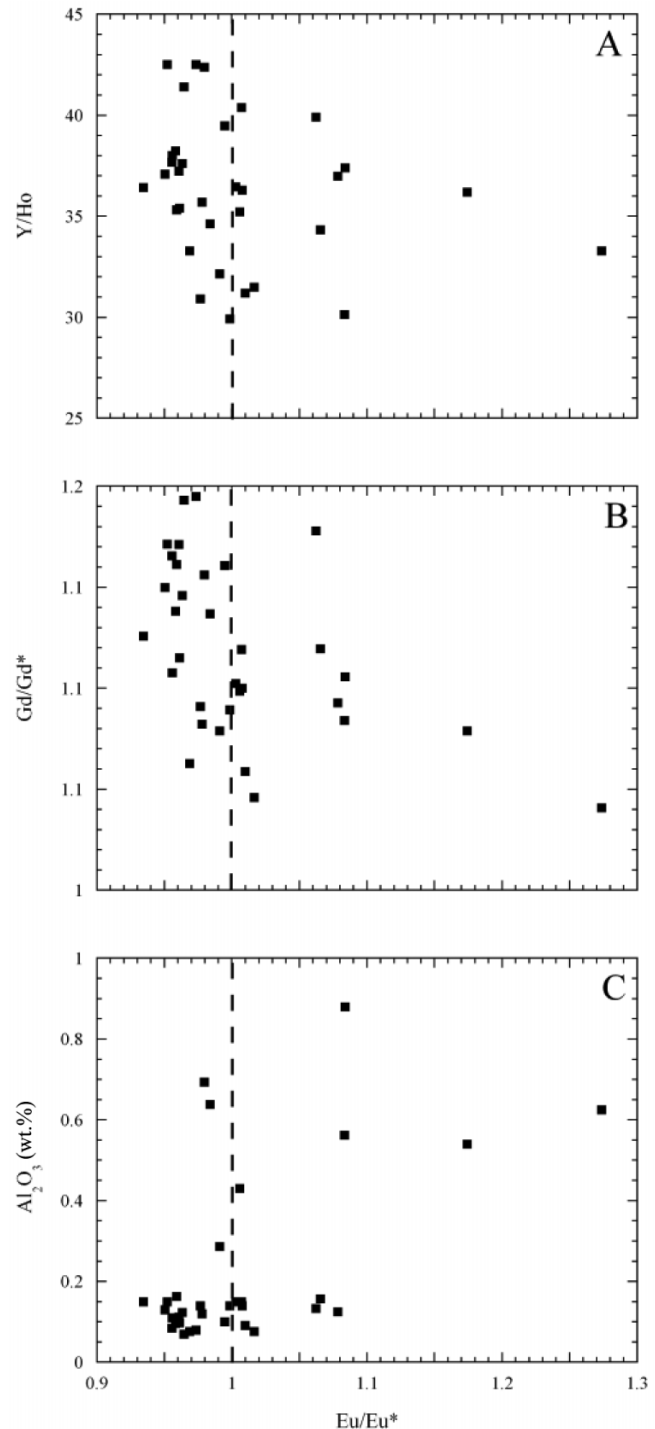
The final REE+Y feature associated with seawater is a positive La anomaly. Lanthanum is fractionated from its neighbouring REE because of its empty 4f-orbital, which limits adhesion to particles during the introduction of dissolved REE from freshwater into the marine system (Bau 1996, 1999), thereby causing it to be overenriched in seawater, and in hydrogenous precipitates that form in equilibrium with seawater (e.g., Bolhar et al. 2004). Samples from the Rapitan iron formation, however, do not consistently produce positive La anomalies. The surprising finding is that several samples ($n = 8$) have La/La* values <1, or in other

Fig. 8. Histogram showing the distribution of La/La* (see Lawrence et al. 2006 for formula) values normalized to MuQ (grey) and the USGS granitoid standard GSP-2 (black). Both have bimodal distributions, but when normalized to GSP-2, the entire data set is shifted into positive La anomalies, whereas the lower mode in the MuQ-normalized data set produces apparent negative La anomalies. No negative La anomalies are known from rocks, and so this finding implies that the local dissolved REE+Y supply originated from catchment areas dominated by LREE-rich rocks, possibly of granitoid composition.
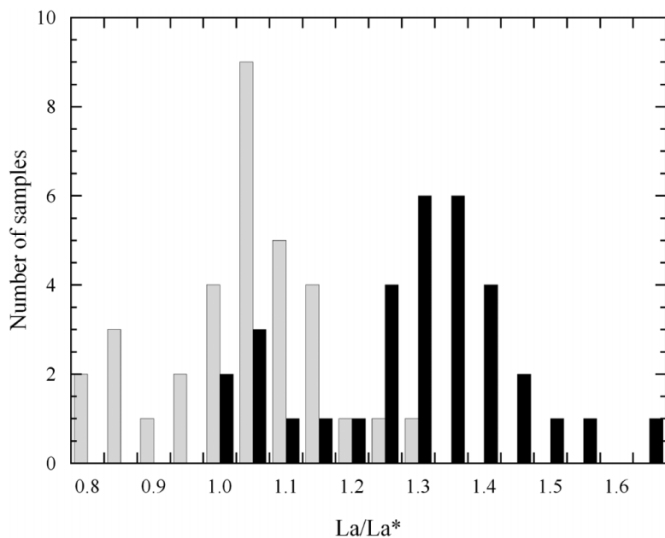
words, slightly negative La anomalies (Fig. 8). This is clear evidence for an artefact of normalization because there are no known processes that can negatively fractionate La from the other LREE. When a water body is under the influence of a local, very LREE-enriched source, normalization to average upper crust may not show a La anomaly (Kamber et al. 2004). This is in part because the MuQ upper continental crust composite is from a drainage that samples heavily from an intraplate basalt province, and is not especially enriched in the LREE, and thus normalization to a local granitic source may be more appropriate for the Rapitan Basin. The drainage area of the Rapitan Basin is poorly constrained, but to explore the possibility of a granitic catchment, the data were normalized to the USGS granite standard GSP-2. This pulled all of the La/La* values >1 (La/La* = 1.03–1.65) (Fig. 8), thereby eliminating the seemingly negative La anomalies that had been produced by normal crustal normalization. This solution suggests that a local source of roughly granitic composition may have contributed dissolved REE into the Rapitan Basin. This possibility is supported by the presence of granitic "stranger stones" in the lower Sayunei Formation (Ross and Villeneuve 1997), as well as the abundance of quartz arenite in the Katherine Group of the lower Mackenzie Mountains supergroup (e.g., Long et al. 2008), which was probably produced by the weathering of granitoid rocks on the Canadian Shield and Grenville Province to the east. The quartz arenite was probably the main source of quartz-rich clastic material in the glaciogenic deposits of the Sayunei and Shezal formations, and its subglacial weathering would probably have introduced significant amounts of La into the basin. The influence of a local granitic input is most pro-

nounced in La because in the chert it is the relatively most depleted REE, whereas in the granite, it is the relatively most enriched REE.

The combined analysis of the various REE+Y features suggests that the Rapitan iron formation formed in a basin that received dissolved REE both from the open ocean as well as from local drainage. These two seemingly diametric oceanographic conditions can coexist in partially restricted basins. Such partially restricted basins are referred to as "silled basins", in reference to a subaqueous topographic high that restricts water exchange with the open ocean, while also allowing moderate exchange across shallow water depths.

Mo–U systematics

Two of the most useful features in diagnosing different basin types are the redox conditions and stratification of the water column. These phenomena leave distinctive geochemical signatures in the sediment, which can be used to aid in basin reconstruction. Many of the transition metals have multiple redox states and record oceanic and diagenetic conditions (e.g., Tribovillard et al. 2006). Among the most useful redox-sensitive metals are molybdenum and uranium. Both of these metals exhibit conservative behaviour in modern seawater and have very long residence times. Unlike some other redox proxies, both Mo and U are evenly distributed throughout the open ocean relative to both area and depth, making them more practical tools than many other metals. Molybdenum and U are strongly overenriched in seawater relative to their crustal abundances; Mo is the most abundant transition metal in the modern oxygenated ocean (Algeo and Maynard 2008), but its estimated concentration in the ocean changed significantly over the course of the Precambrian (Scott et al. 2008).

Molybdenum is soluble in oxic conditions as the molybdate ion, MoO_4^{2-}, which is slowly removed from seawater through scavenging by Mn oxides. Under euxinic conditions, it can form thiomolybdate ($MoO_xS_{4-x}^{2-}$; $x = 0–3$), which is highly particle reactive and is scrubbed from the water column at much greater rates though adsorption onto Fe sulphides, Fe and Mn oxides, organic material, and clay minerals (Algeo and Tribovillard 2009). Alternatively, it may form Fe–Mo–S complexes similar to mackinawite under conditions with moderately low dissolved H_2S. These complexes then adhere to larger particles (Helz et al. 2011). Either of these two Mo-fixation methods requires the presence of H_2S in the water column, and thus at least mildly euxinic conditions. Uranium, in contrast, exists in oxic seawater as highly soluble uranyl carbonate $UO_2(CO_3)_3^{4-}$ and is reduced to less-soluble U oxides (e.g., UO_2, U_3O_7, and U_3O_8) under anoxic conditions (Algeo and Tribovillard 2009, and references therein). These more reduced U species are removed from the water column by direct transfer across the sediment–seawater interface and attendant precipitation or slow adsorption, a process quite distinct from those affecting Mo. Besides their preferred fixation mechanisms, each of these metals reacts under different redox conditions: U is fixed under all anoxic conditions, completely independent of the presence of dissolved sulphide, whereas Mo requires at least mildly euxinic (i.e., sulphidic) conditions (Morford and Emerson 1999; Morford et al. 2005; Tribovillard et al. 2006; Algeo and

Maynard 2008; Algeo and Tribovillard 2009). The characteristic redox pathways make the enrichment of these two metals relative to one another an excellent geochemical tool in basin analysis.

Although most of the systematics for the redox behaviour of Mo and U have been worked out using a combination of modern redox-sensitive basins and Paleozoic shales, the basic principles of their behaviour should be similar for iron formation environments. Due in large part to the limited number of modern analogues for an iron-rich basin (e.g., Crowe et al. 2008b; Mikucki et al. 2009), the behaviour of these metals must be extrapolated from these other, better understood systems. Although several factors may directly influence their fixation rates, chiefly the generation of large volumes of iron oxyhydroxides (Tribovillard et al. 2006), our working hypothesis is that the behaviour, and more importantly the relative ratios of the deposited metals, would not be significantly affected.

The role of Mn and Fe oxyhydroxides in the fixation of Mo is fairly well documented (e.g., Algeo and Tribovillard 2009; Goldberg et al. 2009). Because of the ability of Mn oxides, and to a much lesser degree, Fe oxides, to scavenge the molybdate ion from oxic seawater, a strong relationship between these metals, especially in iron formation, may indicate Mo enrichment without euxinic conditions; a strong correlation would suggest that increased Fe deposition controlled Mo fixation rather than changes in the redox conditions of the basin. The lack of any strong correlation between Mo and Fe_2O_3 (Fig. 9A), across the full range of compositions, demonstrates that iron deposition rates were not a limiting factor in Mo enrichment, although the development of a correlation in midrange concentrations of both Mo and Fe_2O_3 suggests that an iron particulate shuttle was an important but not limiting factor. Furthermore, Mo shows no correlation with MnO (Fig. 9B), essentially eliminating the possibility of a particulate shuttle that fixed Mo as molybdate, and that some free H_2S was needed to drive Mo fixation. Although it could be argued that a Mn oxide was still the driving factor in Mo shuttling across a redoxcline through subsequent Mn reduction, dissolution, and Mo release in anoxic bottom waters (e.g., Algeo and Tribovillard 2009), such a possibility can be eliminated because of the absence of a positive Ce anomaly, as discussed earlier in the text. The high reactivity of Mo–S compounds allows easy adhesion to clay particles, organic material, or even amorphous silica colloids, as well as to the more widely discussed Fe oxides. All of these, in varying amounts, would have been significant components of any particle shuttle operating during the deposition of the Rapitan iron formation.

One of the limitations commonly faced when using redox-sensitive trace metals as paleoredox proxies is that detrital sediment supplied to the basin can mask the concentrations contained in authigenic phases. Several approaches have been employed to address this issue, most commonly the normalization of the metal of interest to Al, expressed as the [metal]/Al ratios (e.g., Morford and Emerson 1999; Lyons et al. 2003; Cruse and Lyons 2004; Tribovillard et al. 2004). The same approach has also been applied using other immobile trace elements, such as Th (e.g., Meyer et al. 2008; Pollack et al. 2009). Such straightforward correction fails to illustrate properly the true degree of authigenic enrichment

Fig. 9. Covariance diagrams of elemental Mo (ppb) and Fe_2O_3 and MnO (wt.%). (A) Molybdenum does not correlate with Fe_2O_3, indicating that increased iron deposition did not directly influence Mo fixation rates, although the strong correlation for samples at mid-range Mo and Fe_2O_3 concentrations suggests that iron particles may have nonetheless been an important particle shuttle for Mo at moderate concentrations. (B) No correlation between Mo and MnO is seen, indicating that a Mn particulate shuttle was not a factor in Mo fixation.
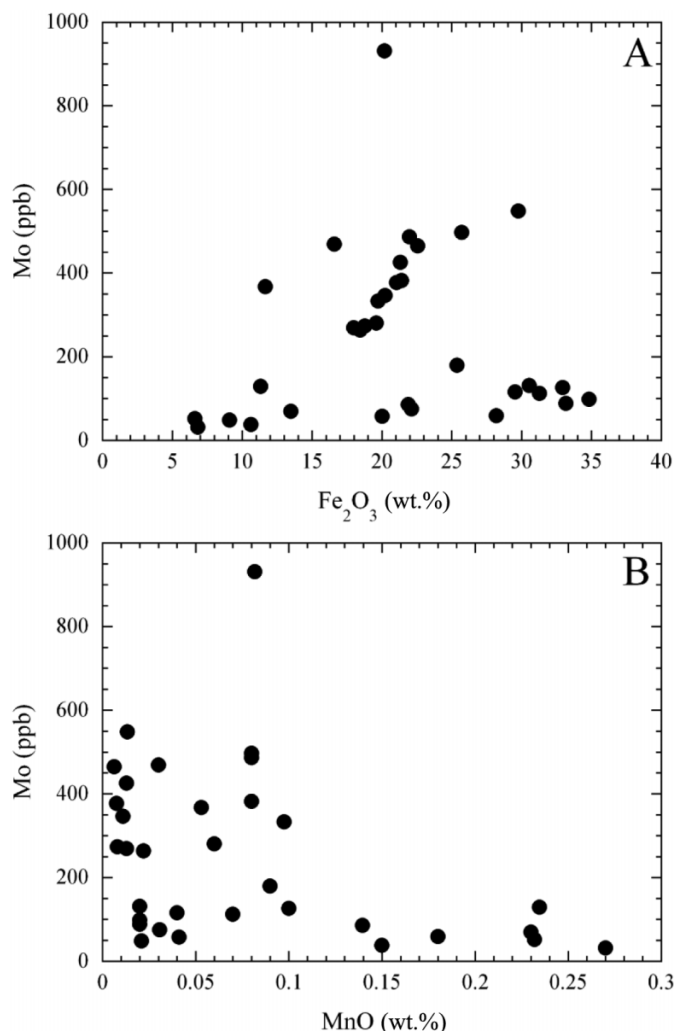
in many sediments (Van der Weijden 2002). For example, although Th is of great utility when assessing U, because of their strong relationship, it becomes ineffective when comparing the enrichment of U with a metal with dissimilar behaviour, such as Mo, thus necessitating the use of an element whose behaviour differs from that of both Mo and U. Simple Al normalization can also produce inaccuracies if the sediment contains a very small detrital component or exceedingly low Al concentrations relative to other immobile elements, such as Ti (e.g., Tribovillard et al. 2006). An alternative approach is double normalization to a shale standard and an immobile element (e.g., Van der Weijden 2002; Meyer et al. 2008; Algeo and Tribovillard 2009). Such an approach can establish the degree of enrichment over crustal averages, expressed as unitless "enrichment factors" (EF) as described, for example, by Algeo and Tribovillard (2009). These calcu-

lations most commonly use Al as the detrital proxy, and the Post-Archean Australian Shale (PAAS) of Taylor and McLennan (1985) as the shale standard. The standard used in the present work is MuQ (Kamber et al. 2005) because it, unlike shale, provides an upper-crustal average that has not been influenced by diagenesis. The original alluvial sediment data set from which MuQ was calculated lacks Mo data, but this has been supplemented with a much larger, new data set for similar alluvial sediment, with an average Mo content of 485.3 ppb from Marx and Kamber (2010). Aluminum is used as the proxy for the detrital component because it demonstrates a hyperbolic correlation with both Mo and U, whereas other immobile elements (e.g., Sc, Ti, Ga, Zr, Nb, Th) were less consistent in this regard. Several of the other possible normalizers were rejected for reasons such as strong correlations with U, but not Mo (Zr, Th), unusually high Nb/Ta ratios, and commensurately strong correlations between Ti and both Nb and Ta, suggesting that these three elements are controlled by the same mineral phases in this depositional environment. Both U and Mo show weak relationships with loss on ignition (when available), indicating that neither is strongly related to low-Al phases such as carbonate or organic carbon, which also addresses the concerns expressed by Van der Weijden (2002) regarding Al normalizations.

The enrichment factors of several metals are plotted against stratigraphy in Fig. 10. Each of these metals (Mo, U, W) shows distinct stratigraphic variation relative to the others. Mo and U do not show strong covariance with respect to stratigraphy, and U enrichment, although somewhat variable, averages to a fairly constant low enrichment throughout the section. This is to be expected because U is removed from the water column at steady rates under anoxic conditions and would show sustained changes in its authigenic enrichment only during intervals of oxia. Therefore, it can be inferred that anoxic bottom water prevailed for the duration of iron formation deposition. Molybdenum is most strongly enriched in the lowermost and uppermost parts of the iron formation stratigraphy. This distribution indicates sulphidic (euxinic) conditions were present in the water column during deposition of strata at the base and top of the iron formation, but were absent during the middle of the depositional interval, where Mo enrichment is closer to presumed background levels.

The aqueous behaviour of W under reducing conditions is poorly understood (Johannesson et al. 2000; Seiler et al. 2005), but its systematics in the studied Rapitan section are included here to show that it demonstrates transitional behaviour between Mo and U. The relationship between Mo and W in numerous other systems, including microbiology, is well documented (Kletzin and Adams 1996; Arnórsson and Óskarsson 2007). The biogeochemical behaviour of these elements is also known to be somewhat similar to that of V, another redox-sensitive trace metal (Johannesson et al. 2000). Under oxic conditions, W behaves very much like Mo, but it does not react with H_2S under euxinic conditions (Arnórsson and Óskarsson 2007). This apparent resistance to forming sulphides, despite the similarity of the valence states of W and Mo, may help to explain why the stratigraphic distribution of W enrichment is transitional between that of Mo and U. Caution must be used in applying this insight, however, until the aqueous redox behaviour of this metal is better constrained.

Fig. 10. Stratigraphic distributions of the enrichment factors (EF) for Mo, U, and W. Stratigraphic column on the left is the iron formation interval from Fig. 3. Molybdenum is significantly more enriched in the upper and lower parts of the iron formation, indicating stronger mechanisms for Mo fixation, whereas U is more constant throughout the section. Tungsten is transitional between Mo and U, showing relative enrichment at the base and top of the section like Mo, albeit with much smaller enrichment factors. See text for further discussion.
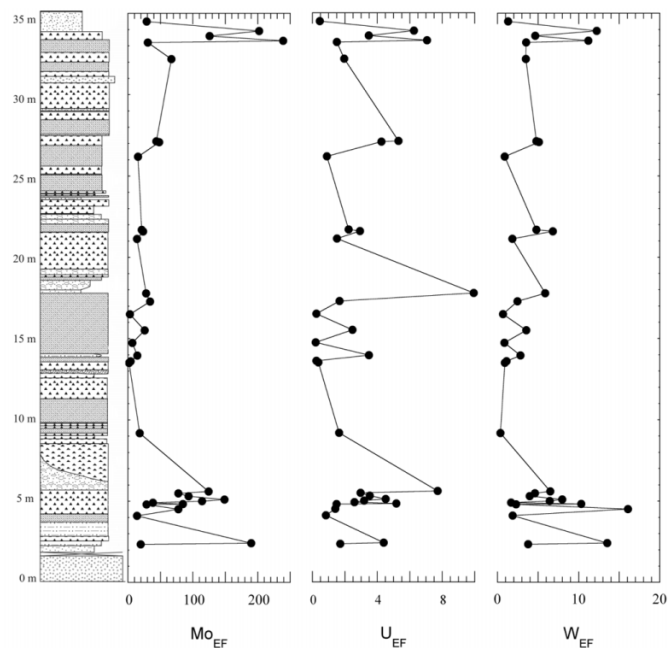

Fig. 11. Covariance plot of Mo_{EF} and U_{EF}. These elements show good covariance, with stronger absolute enrichment of Mo than U. Similar relationships exist between both of these metals and Ni, Co, Pb, and Sb, but not with V. Dotted lines show the expected trends in the Mo_{EF}–U_{EF} space for the modern Cariaco Basin (C.B.), Black Sea (B.S.), and Eastern Tropical Pacific (E.T.P.). EF, enrichment factors.
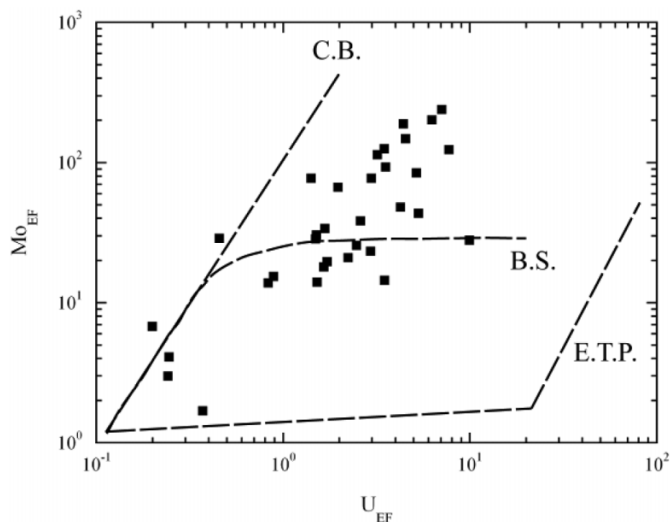
The distinct redox behaviours of Mo and U makes plotting these two elements against one another of great utility for evaluating basinal redox conditions and basin configuration. This can be done most effectively using their enrichment fac-

tors (Fig. 11). The relatively tight clustering and well-developed trend demonstrates the effectiveness of this approach, as compared with plots of absolute Mo versus U concentration, which show considerable scatter in a broad, fan-shaped array. The trend formed by the enrichment factors rises with a steep slope from the origin with relatively little deviation. Many other redox-sensitive elements, including W, Ni, Co, Sb, and Pb, are similarly correlated with either Mo or U, although V does not correlate with either element. Reconstruction of the Rapitan Basin in the following section will focus on the established correlation between Mo and U and the REE+Y systematics because their behaviour in the modern setting is well understood.

Basin reconstruction

Using Mo_{EF} versus U_{EF} covariance plots, Algeo and Tribovillard (2009) were able to distinguish three types of modern redox-sensitive basin: (i) zones of marine upwelling and high primary productivity (e.g., Eastern Tropical Pacific); (ii) highly restricted basins (e.g., Black Sea); and (iii) partially restricted, silled basins (e.g., Cariaco Basin). Each of these basin types develops a distinct Mo_{EF} versus U_{EF} trend that is controlled by a combination of the redox stratification and evolution of the basin, the degree of connectivity with the open ocean, and the refreshing rate of the basinal waters.

Highly restricted basins

The most distinctive of the three modern basin types, the highly restricted Black Sea, typically forms Mo_{EF} versus U_{EF} trends that are flat overall, showing greater U enrichment over Mo, although at near-constant elevated Mo enrichment. This is because such highly restricted basins develop long-term, persistent euxinia at depth, which promotes the reduction of molybdate to thiomolybdate, and thus elevates Mo removal rates from seawater. Over time, a reservoir effect develops, in which Mo, through prolonged drawdown in the euxinic parts of the basin, becomes supply limited. This effect also implies pronounced basin restriction that limits mixing of the basin water with the open ocean to only the shallowest water depths, and even then with only limited water-mass exchange. In contrast, U does not develop a significant reservoir effect because of its steady fixation rate, and it continues to be enriched well after the Mo supply has been depleted. This allows for the development of flat Mo_{EF} versus U_{EF} trends with somewhat elevated Mo enrichment (Algeo and Tribovillard 2009; Fig. 11, B.S.). The much steeper slope shown in the Rapitan samples indicates that the Rapitan Basin was not nearly as restricted as the modern Black Sea. A highly restricted basin was already considered unlikely based on the REE+Y data, which indicate considerable connectivity with the open ocean, showing consistently elevated Y/Ho ratios, positive Gd/Gd* values, and a strongly developed positive REE slope overall.

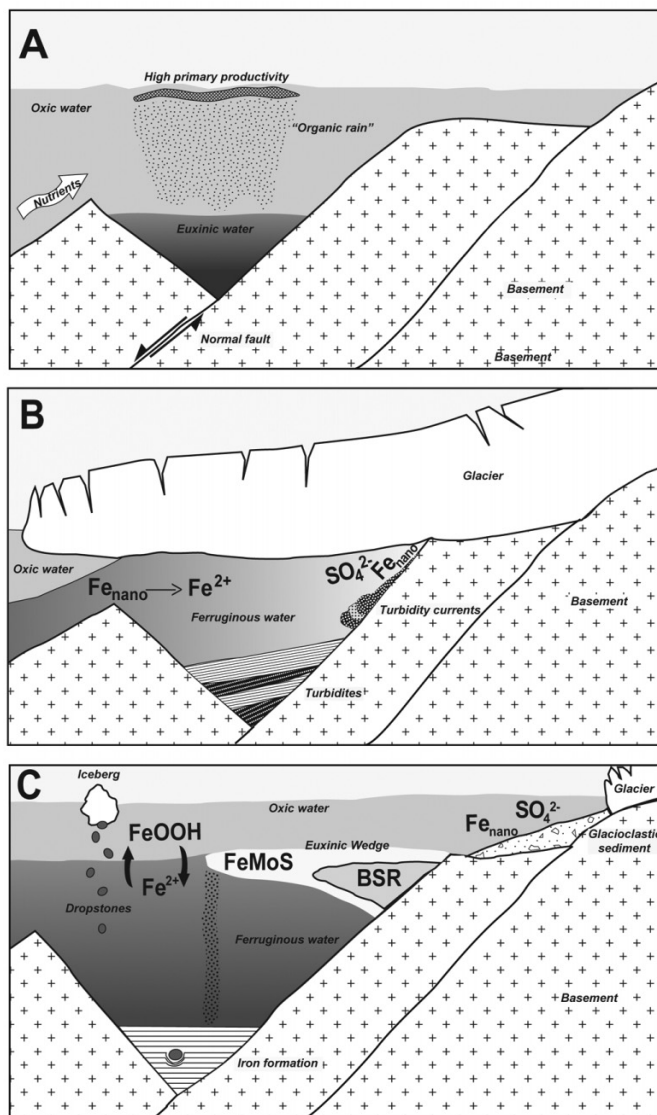### Zones of upwelling and high productivity

At the other end of the spectrum are open-marine settings characterized by deep-water upwelling that causes high primary productivity near the top of the water column, such as in the Eastern Tropical Pacific along the western coasts of North and South America. Nutrient-rich deep water is up-welled into the photic zone in these areas, creating a bloom in biological activity. This increased productivity results in prolific export of organic material to the seafloor, the decomposition of which causes anoxic conditions to develop in sediment pore waters and, rarely, in seawater just above the sediment–seawater interface (e.g., Morford et al. 2005; Pattan and Pearce 2009). Uranium is commonly markedly overenriched relative to Mo in sediment from these areas because suboxic to anoxic bottom and pore waters are sufficient to cause its enrichment. Water-column euxinia is rare in these zones because O_2 deficiency is generally limited to pore waters, where it is not sufficient to promote Mo removal from the water column. The combined effect leads to shallow slopes on Mo_{EF} versus U_{EF} diagrams for most sediment deposited in these environments (Algeo and Tribovillard 2009; Fig. 11, E.T.P.). These trends are different from that of the Rapitan iron formation. In the rare occurrence of water-column euxinia in an upwelling zone, steep Mo enrichment can develop, but the steep trend in such a situation would trend away from already elevated U enrichment levels because of persistent U enrichment in all conditions, whereas the trend discovered in this study extends from the origin. This suggests that the Rapitan Basin was probably not a zone of oceanic upwelling and high productivity. The REE+Y patterns also suggest a degree of restriction in the system, which is inconsistent with this type of redox-sensitive marine area. Consequently, a basin as open to the global ocean as this can be eliminated from consideration for the Rapitan Basin.

Silled basins

The third type of redox-sensitive environment is a partially restricted, "silled" basin, such as the Cariaco Basin off the Caribbean coast of Venezuela. This basin type features a deep-water depression protected by a series of bathymetric highs ("sills"), that limit mixing of the deepest waters of the basin with the open-marine realm, while allowing most of the water column to remain well mixed with the open ocean (Lyons et al. 2003). Silled basins are distinct from Black Sea type basins because the latter are almost completely cut off from the open ocean at depth, and experience only limited exchange of surface waters, whereas silled basins have full connectivity at all but the deepest parts of the basins (Fig. 12A). If a pronounced redoxcline is established, silled basins can develop long-term euxinia in their bottom waters, which allows for the fixation of Mo through the generation of Fe–Mo–S compounds of variable stoichiometry (Helz et al. 2011). Unlike the Black Sea, however, the high connectivity of the upper parts of the water column helps prevent Mo exhaustion because the metal budget of the euxinic bottom waters can be maintained through slow exchange across the redoxcline, episodic spillover of extrabasinal ocean water, or a Mn/Fe particulate shuttle. The nearly constant Mo supply in these systems allows for steep Mo enrichment relative to U, which is fixed at the same rates as in any other redox-sensitive basin (Algeo and Tribovillard 2009; Fig. 11, C.B.). The steep slopes in the Mo_{EF} versus U_{EF} covariance plots generated by modern basins of this type is closely mirrored by the slope defined by the Rapitan iron formation, indicating that the Rapitan Basin may have been similarly silled. The REE+Y systematics, which also indicate a hybrid source of dissolved species, further support this basin type.

Fig. 12. Schematic diagrams of three partially restricted basin models for a rift basin setting. (A) In the classic silled basin model, based on the Cariaco Basin (after Lyons et al. 2003), a bathymetric sill, formed, for example, by a down-dropped fault block, limits water exchange between the deep basin and the open ocean, with stratification controlled by the development of a chemocline. The upper water mass has unrestricted exchange with the open ocean, allowing for a steady supply of dissolved metals to the basin. This model cannot be applied directly to the Rapitan Basin because it does not account for ice cover. (B) In a rift basin with widespread ice cover, free oxygen in the upper water column of the basin would be limited, allowing the preexisting ferruginous deep water to become the dominant redox state of the basin. During this time, clastic sediment and dissolved sulphate produced by limited chemical weathering beneath a wet-based glacier would be introduced into the basin through subglacial outwash, depositing the thick turbidites of the lower Sayunei Formation and raising the dissolved sulphate concentration in the basin to glauberite saturation. Simultaneously, glacially derived, highly reactive iron oxyhydroxide nanoparticles (Fe_{HR}) would be introduced into the basin and reduced to soluble Fe^{2+} by iron-reducing bacteria, gradually increasing the dissolved iron content in the ice-capped basin to levels that could deposit iron formation. (C) Upon glacial retreat from a previously ice-covered rift basin and exposure of the basin water to atmospheric oxygen and sunlight, high primary productivity occurs, generating sufficient organic material in anoxic shallow to middle water depths to initiate bacterial sulphate reduction (BSR) and produce a mildly euxinic "wedge" in middle water depths. Dissolved MoO_4^- is converted to Fe–Mo–S compounds at relatively low H_2S concentrations, which adsorb to the surface of flocculating iron oxyhydroxides that form through the oxidation of dissolved Fe^{2+} in the oxic upper water column. The relative position of the wedge dictates either strong Mo enrichment (solid line) or weaker enrichment (dashed line). The basinal iron supply may be refreshed through the input of additional glaciogenic Fe_{HR} nanoparticles, or via upwelling of nonhydrothermal iron from extrabasinal sources. Iron formation deposition occurs only during sea-level highstand, when most glaciogenic clastic sediment is trapped in shallow, proglacial estuaries. At this time, the primary source of clastic sediment to the basin is dropstones from icebergs.

The basin configuration emerging from the geochemical data is consistent with the basinal architecture that was established using sedimentological and stratigraphic evidence. The Rapitan Group was deposited in an incipient rift basin (Yeo 1981; Eisbacher 1985), a dynamic tectonic setting that is capable of producing bathymetric sills, such as the uplifted edges of graben systems. The geologically ephemeral tectonic regime of a rift system could also limit the longevity of the silled basin through continued rift subsidence. This may help to explain why iron formation was deposited during only a brief stage of Rapitan Group deposition and why thick iron formation is of limited geographic extent. It also helps explain why the Rapitan Group is divided into a series of sub-basins across the Mackenzie Mountains (Yeo 1981). The limited distribution of iron formation within each sub-basin also conforms to the typical view of rift systems, which commonly consist of a series of topographic lows that are not necessarily well interconnected.

Nature of the redox chemocline

A drawback of using the modern silled basin model for the Rapitan Basin is that one of the most important processes in such basins today is the role of a Mn-oxide particulate shuttle. In the modern Cariaco Basin, apart from intermittent spillover of water from the open ocean into the basin, the principal mechanism for the transport of Mo and other metals into the euxinic zone is through Mn redox cycling (Algeo and Tribovillard 2009). In modern basins, the oxidation of dissolved Mn^{2+} to Mn oxyhydroxides occurs in the oxic zone. Molybdate ions readily adsorb to Mn oxides, providing the primary mechanism for Mo removal from oxic seawater (Morford and Emerson 1999; Morford et al. 2005; Tribovillard et al. 2006). In a stratified basin in which the upper water column is well connected to the open ocean, Mn oxides would readily form in the upper water column, but would redissolve upon settling below the redoxcline into more reduced waters, releasing all adsorbed material such as Mo and Ce. This process keeps the metal supply in these basins almost constant and can lead to overenrichment of some metals in the anoxic bottom waters (Algeo and Tribovillard 2009; Planavsky et al. 2010a). Strong evidence against this

process is present in the Rapitan Basin: one of the characteristic signs of this process is a positive Ce anomaly, a phenomenon documented in some late Paleoproterozoic iron formation and in bottom waters from modern redox-sensitive basins, but not present in the Rapitan, where normalized Ce is either flat or shows a slight negative anomaly. The absence of a Mn shuttle does not preclude the silled basin model: the oxidation of dissolved Mn^{2+} to Mn oxyhydroxides is common in modern settings but, because of the complexities of the redox and chemical state of the Neoproterozoic ocean, may not have been in effect at that time.

An iron particulate shuttle across an oxic-ferruginous redoxcline was probably in operation in the Rapitan Basin, as opposed to a Mn-oxide shuttle. This process would not generate a positive Ce anomaly, but would allow for a nearly constant marine metal budget in the suboxic to anoxic watermasses. Redox stratification of the basin during deposition of the Rapitan iron formation was a critical component of the classic depositional model of Klein and Beukes (1993). The nature of the redox stratification in that model is, however, overly simplistic. Given that significant Mo enrichment relative to U requires at least mildly euxinic conditions, it can be inferred that the Rapitan Basin had at least three different water masses, defined by their redox conditions. Euxinic water in the basin would have been, by necessity, quite limited in extent. To generate large volumes of ferric iron oxides (hematite or its precursors), much of the basin, including the bottom waters, must have been under ferruginous conditions and transitioning towards oxic conditions because pervasive euxinia would promote the formation of pyrite and inhibit the buildup of sufficient dissolved ferrous iron to generate iron formation. Consequently, the Rapitan Basin was highly redox-stratified, and probably consisted of oxic surface waters, highly ferruginous deep waters (iron enrichment of sufficient levels to form large iron formations), and intermittent, weakly euxinic middle water depths. This type of stratification differs strongly from most modern redox-stratified basins, such as the Black Sea and Cariaco Basin, and more closely resembles ferruginous lakes, such as Lake Matano, Indonesia (Crowe et al. 2008b), of which there are far fewer modern examples.

Nature of the sill

A major difference between the Rapitan and Cariaco basins, besides the established redox water column stratigraphy, is the largely unknown influence of ice cover. Capping of the ocean by thick sea ice, as would have been the case in the classic model for snowball Earth (e.g., Kirschvink 1992; Hoffman et al. 1998; Hoffman 2009), plays a major role in the BIF model of Klein and Beukes (1993). Evidence for the presence of glaciers and either sea ice or an ice shelf is present throughout the Rapitan Group, in the form of diamictites and abundant dropstones in the iron formation. The full scope of the influence of sea ice on the redox stratification in a Neoproterozoic basin remains to be fully explored. Currently, the most detailed proposal hypothesizes that prolonged ice cover would promote stagnation and the buildup of dissolved ferrous iron in the basin waters (e.g., Klein and Beukes 1993). Furthermore, in a modern example of subglacial stagnation from Antarctica, in the McMurdo dry valleys, strong redox stratification develops in some of the subglacial

lakes. There, the REE+Y evidence points towards a Mn particulate shuttle, as demonstrated by positive Ce anomalies observed at depth (De Carlo and Green 2002). Other basins in the region have developed high concentrations of dissolved ferrous iron, primarily through anaerobic bacterial activity and complete isolation from the atmosphere and ocean, and have been suggested as possible analogues to Neoproterozoic basins that contain iron formation and glaciogenic siliciclastic rocks (Mikucki et al. 2009). These modern examples are imperfect analogues because they are lakes, not restricted oceanic basins, but they do help to demonstrate that glacial ice can induce water column stratification and redox stagnation.

The redox stratigraphy of modern basins is maintained through the formation of hydrological barriers that are generally independent of the redox state of the basin. These are most commonly temperature gradients (thermocline) and salinity gradients (halocline). These features commonly occur together, as is the case in the Cariaco Basin, where colder, more saline water underlies a combined halocline and thermocline that forms the barrier between oxic and anoxic water (Lyons et al. 2003). Either of these features is easily formed in a glaciomarine environment, where glacial outwash injects cold, fresh water into the basin, commonly contributing to the formation of either a thermocline or halocline (although such a system would be associated with clastic sedimentation that would inhibit the deposition of chemogenic iron formation). This process could allow for the development of glacially triggered water-column stratification, which when coupled with basin restriction would aid in preservation of strong redox stratification of the water column, and greatly inhibit mixing and dilution of distinct basinal water masses.

To maintain long-lived redox stratification in a basin, physical barriers between the deeper basin water and the open ocean are needed. As discussed earlier in the text, active movement along normal faults (Helmstaedt et al. 1979) during Rapitan deposition associated with early rift formation could easily have generated a well-defined sill along the rift margin. Furthermore, because there was active subsidence and rifting, continued movement along the normal faults would maintain accommodation space in the basin over much longer intervals and would prevent the basin from shallowing and gradually increasing its overall degree of connectivity to the open ocean.

New model for Neoproterozoic iron formation

The presence of ice-transported sediment in the Rapitan Basin clearly limits the extent to which the Cariaco-type silled basin model can serve as an analogue for the Neoproterozoic because sea ice has the ability to isolate the system from the atmosphere and possibly from the open ocean. Any proposed model for the Rapitan Basin must therefore consider the effect of ice. A bathymetric sill, formed by a hanging-wall block, is without question capable of creating a partially restricted basin. The structural and sedimentological evidence for a rifted graben environment also helps to explain the geographically variable thickness of iron formation throughout the Rapitan Group exposure area. However, the relative roles of ice-capping versus bathymetric sill in promoting the buildup of sufficient iron to deposit the thick iron formation unit of the Snake River region are difficult to assess.

Here we envisage a silled basin that, during extended intervals of ice cover and concomitant sea-level lowstand, would have been isolated from the atmosphere and restricted from the open ocean (Fig. 12B). At times, the basin could have been completely isolated from the ocean, when the thick ice shelf was grounded on the sill at the outboard edge of the basin. Isolation from the atmosphere, as well as inhibition of photosynthesis due to ice cover, would have resulted in the rapid drawdown of free oxygen in the shallow water column, allowing ferruginous conditions, already prevalent in the deep basin (e.g., Johnston et al. 2010), to become the dominant redox state at all water depths (Fig. 12B). During this time, large amounts of clastic material would have been introduced to the basin through subglacial outwash, generating fine-grained turbidite deposits. In our model, this is the setting in which the turbidite-dominated Sayunei Formation (Yeo 1981) was deposited. In addition to clastic sediment, there would have been a small supply of dissolved sulphate generated through oxic weathering of sulphide-bearing rocks and mechanical weathering of sedimentary sulphates under the wet-based glacier. Because of low productivity levels, the dissolved sulphate would have gradually built up to saturation levels, causing the precipitation of small amounts of sulphate minerals, such as glauberite (now preserved as dolomite pseudomorphs), within clastic strata (Young 1976). In addition to clastic material and sulphate, glaciers have been documented as the dominant iron supply to the modern open ocean (Raiswell et al. 2006). Thus, it can be envisaged that highly reactive ferric iron oxyhydroxide nanoparticles such as lepidocrocite (Fe_{nano}), which are both readily bioavailable and easily reduced and dissolved under ferruginous marine conditions, were supplied by the ice sheet (Fig. 12B). Iron-reducing bacteria have been documented in modern ice-capped, restricted basin settings, such as Blood Falls, Antarctica (Mikucki et al. 2009), where they reduce these particles to ferrous iron while autorecycling sulphur and carbon, allowing for minimal organic carbon burial and H_2S production. Prolonged intervals in which such microbially mediated iron reduction was taking place would have enabled the buildup of enough dissolved iron in the basin to eventually form the large iron deposits of the Snake River region. Additional iron could also have entered the basin through limited exchange with ferruginous seawater from the deep open ocean (Fig. 12B).

Upon glacial retreat and subsequent sea-level rise, the iron-rich basin waters would have become simultaneously exposed to both atmospheric oxygen and sunlight (Fig. 12C). Because of the relatively high concentration of nutrients, such as Fe^{2+}, and SO_4^{2-}, which had been able to build up in the basin during ice cover, primary productivity in the upper water column would have exponentially increased, resulting in the rapid sequestration of large volumes of organic carbon in shallow to middle water depths. Burial of this carbon, combined with the elevated dissolved sulphate concentrations in the water column, would have enabled bacterially mediated sulphate reduction (BSR) to generate sulphidic conditions in deeper shallow to median depth water, generating a euxinic wedge that migrated outwards from the lower shelf to upper slope. This condition is similar to what has been proposed in several recent models for other intervals in the Paleoproterozoic

and Neoproterozoic (e.g., Johnston et al. 2010; Li et al. 2010; Poulton et al. 2010; Poulton and Canfield 2011).

During times of maximum BSR, the euxinic wedge would extend far out into the basin along the chemocline between oxic surface waters and ferruginous deep water. It is unlikely that this wedge would ever have been strongly euxinic, owing to the large amount of Fe^{2+} in the water column, which would have generated large quantities of iron sulphides and quickly exhausted the supply of dissolved H_2S. Importantly, however, strong euxinic conditions may not be necessary for Mo fixation. According to new models for Mo fixation, strong Mo removal under euxinic conditions can occur at much lower H_2S concentrations than previously suggested, through the formation of Fe–Mo–S compounds in lieu of the generation of thiomolybdates, as is the traditionally accepted mechanism for Mo fixation in euxinic environments (Helz et al. 2011). In this model, Mo removal from the water column is primarily dependent on the availability of ferrous iron and pH, with dissolved H_2S merely needing to be present to remove dissolved MoO_4^{2-} from the water column. It has been suggested that Mo fixation can be driven by iron removal alone (Crowe et al. 2008*a*), but in that example the zone of strongest Mo removal corresponds with that of the highest concentrations of H_2S. When applying these new findings to our model for the Rapitan iron formation, we propose that Fe–Mo–S compounds would have been shuttled from the euxinic wedge in middle water depths by newly oxidized iron oxyhydroxides that had formed through the upwelling of dissolved ferrous iron into the oxic surface waters and its subsequent oxidation (Fig. 12C). The iron supply to the basin would been quickly drawn down through the progressive oxidation of the water column, although there may have been continued refreshment of dissolved Fe^{2+} through either upwelling of nonhydrothermal iron from deep waters outboard of the sill, or through the continued supply of Fe_{nano} into the basin by the combination of glacial outwash and icebergs (Raiswell et al. 2006), whose presence can be inferred from the abundant dropstones in the iron formation (Fig. 12C). Larger iron resupply events would have happened during colder times in which persistent sea ice, or potentially ice-shelf readvance, caused the basin to become isolated from the atmosphere again, which may be recorded by the thin interbeds of siltstone in the iron formation.

It is important to note that the basin configuration and water chemistry during deposition of the ferruginous clastic rocks of the Sayunei Formation and the chemogenic iron formation may not have been dramatically different;, the main or only difference may have been the supply rate of clastic sediment. The turbiditic rocks of the lower Sayunei Formation have a very high Fe content (average 12.4 wt.% Fe_2O_3; Yeo 1981), but clastic supply was very high. By contrast, to deposit true iron formation, clastic sedimentation had to be nearly or completely shut off in the deep basin (Klein and Beukes 1993). Here we envisage that because of the sea-level highstand that followed glacial retreat, much of the clastic sediment deposited in the proglacial environment would have been trapped in shallow water on the upper shelf (Fig. 12C). The combination of rising sea level, isostasy, and subsidence along rift-margin normal faults would prevent significant volumes of clastic material from reaching the deep basin. Consequently, with the exception of the delivery of coarse

material into the basin in the form of ice-rafted debris, drop-stones, and infrequent, brief episodes of silt and fine sand-stone deposition (distal turbidites), chemical sedimentation would dominate in the deep basin, allowing for the formation of large volumes of "true" hydrogenous iron formation. The most probable cause for the termination of iron formation deposition is, therefore, the loss of accommodation space. As other authors have reported, the top of the iron formation locally contains granular iron formation (GIF), which is evidence of shallow-water deposition (Klein and Beukes 1993), and is overlain by ferruginous glacioclastic rocks. This suggests that although the dissolved iron supply locally remained high well after the end of iron formation deposition, shallowing water, and eventually clastic sedimentation, drove the cessation of hydrogenous iron formation deposition.

Oxidation state of the Neoproterozoic open ocean

The REE+Y patterns in the Rapitan iron formation are a combination of open-marine and local (LREE-enriched) sources. The strong correlation of REE+Y features is not a function of terrigenous contamination but probably reflects varying importance of the two major dissolved REE+Y sources to the basin. The data thus suggest variable connectivity with the open ocean. The most surprising finding in this regard is the absence of a positive Eu anomaly in most Rapitan samples. If, as is widely postulated, the late Neoproterozoic deep ocean was sulphidic or ferruginous, it would clearly be expected that high-temperature hydrothermal vent fluids would have imparted a positive Eu anomaly to the ocean water. However, the Rapitan iron formation lacks such an anomaly, suggesting that the open ocean may already have been quite well oxygenated by the late Neoproterozoic.

The few other published REE patterns for Neoproterozoic iron formations (e.g., Lottermoser and Ashley 2000; Klein and Ladeira 2004) from different localities (e.g., South Adelaide Geosyncline, South Australia; Urucum district, Brazil) also lack evidence for positive Eu anomalies, although this is not readily evident in those studies because of incomplete REE data. The missing anomaly is significant. According to the widely cited theory that for most of the Proterozoic, the deep ocean was sulphidic (i.e., stagnant Mesoproterozoic to Neoproterozoic ocean), hydrothermally sourced iron would be expected to be removed from the water column through the formation of pyrite (Canfield 1998), and the REE would remain dissolved (Bau and Dulski 1999). Sequestration of REE into pyrite would be unable to match the dissolved hydrothermal REE flux into the ocean, and so the ocean as a whole would carry a significant positive Eu anomaly, as did the Archean ocean, for which this phenomenon is well established. Similarly, widespread ferruginous conditions in the open ocean would also preserve the Eu anomaly because hydrothermal REE would stay in solution as long as the iron did, suggesting that even suboxic, ferruginous conditions in the Neoproterozoic open ocean were implausible. The absence of the Eu anomaly requires widespread oceanic ventilation at the time of Rapitan Group deposition. This conflicts with Mo concentration data from black shales, which remained very low until *after* the Neoproterozoic glaciations (Scott et al. 2008). The information from the REE and from Mo are mutually inconsistent and will require better study of

the elemental supply to Neoproterozoic iron formations and further studies of Neoproterozoic black shale.

Summary

High-quality trace element analyses of jasper samples from the Rapitan iron formation enable detailed reconstruction of the depositional basin and oceanic conditions. The REE+Y demonstrate that although the basin maintained a considerable degree of water-mass exchange with the open ocean, local REE+Y sources also supplied a significant flux of dissolved load from geologically localized and chemically distinct sources. Collectively, this indicates some degree of basin restriction. The near absence of the Eu anomaly shows that the open ocean was not only Eu deficient but that hydrothermally sourced Fe was not important for the Rapitan iron formation, indicating instead that the primary iron source may have been glacially sourced iron oxyhydroxide nanoparticles that were subsequently bacterially reduced under ferruginous conditions. Evidence from Mo and U suggests that the basin was partially restricted (silled), which is consistent with evidence obtained from the REE+Y. Although the traditional model for silled basins cannot be applied to the Rapitan iron formation without modification, because of the presence of glacial ice, an alternative model proposes prolonged ice-capping of a silled basin, which allowed for the development of strongly ferruginous conditions. Upon ice retreat, this iron-rich basin would be gradually oxidized from above, triggering high primary productivity and eutrophication on the deep shelf and upper slope, establishing a weakly euxinic wedge in middle water depths. Oxidation of upwelling dissolved ferrous iron into ferric iron oxyhydroxides would provide a shuttle for Fe–Mo–S compounds during the intervals of most persistent euxinia, causing Mo enrichments of over an order of magnitude greater than background levels.

This new model for the configuration of the Rapitan Basin and depositional controls on the iron formation suggest that the Neoproterozoic open ocean was at least partially oxygenated, inhibiting the long-distance transport of Eu. Oceanic ventilation is not compatible with the sulphidic Proterozoic ocean model, nor is it compatible with newer models for a ferruginous Proterozoic deep ocean. Furthermore, the close analogies drawn between Archean–Paleoproterozoic iron formation and Neoproterozoic examples, and vice versa, are inappropriate, at least when discussing the iron source.

Acknowledgements

References

Aitken, J.D. 1989. Uppermost Proterozoic formations in central Mackenzie Mountains, Northwest Territories. Geological Survey of Canada Bulletin 368. pp. 1–26.

Aitken, J.D. 1991*a*. The Ice Brook Formation and post-Rapitan, Late Proterozoic Glaciation, Mackenzie Mountains, Northwest Territories. Geological Survey of Canada Bulletin 404. pp. 1–43.

Aitken, J.D. 1991*b*. Two late Proterozoic glaciations, Mackenzie Mountains, northwestern Canada. Geology, **19**(5): 445–448. doi:10.1130/0091-7613(1991)019<0445:TLPGMM>2.3.CO;2.

Alexander, B.W., Bau, M., Andersson, P., and Dulski, P. 2008. Continentally-derived solutes in shallow Archean seawater: rare earth element and Nd isotope evidence in iron formation from the 2.9 Ga Pongola Supergroup, South Africa. Geochimica et Cosmochimica Acta, **72**(2): 378–394. doi:10.1016/j.gca.2007.10.028.

Algeo, T.J., and Maynard, J.B. 2008. Trace-metal covariation as a guide to water-mass conditions in ancient anoxic marine environments. Geosphere, **4**(5): 872–887. doi:10.1130/GES00174.1.

Algeo, T.J., and Tribovillard, N. 2009. Environmental analysis of paleoceanographic systems based on molybdenum–uranium covariation. Chemical Geology, **268**(3–4): 211–225. doi:10.1016/j.chemgeo.2009.09.001.

Arnold, G.L., Anbar, A.D., Barling, J., and Lyons, T.W. 2004. Molybdenum isotope evidence for widespread anoxia in mid-Proterozoic oceans. Science, **304**(5667): 87–90. doi:10.1126/science.1091785. PMID:15066776.

Arnórsson, S., and Óskarsson, N. 2007. Molybdenum and tungsten in volcanic rocks and in surface and <100 °C ground waters in Iceland. Geochimica et Cosmochimica Acta, **71**(2): 284–304. doi:10.1016/j.gca.2006.09.030.

Babechuk, M.G., Kamber, B.S., Greig, A., Canil, D., and Kodolanyi, J. 2010. The behavior of tungsten during mantle melting revisited with implications for planetary differentiation time scales. Geochimica et Cosmochimica Acta, **74**(4): 1448–1470. doi:10.1016/j.gca.2009.11.018.

Baldwin, G.J., Thurston, P.C., and Kamber, B.S. 2011. High-precision rare earth element, nickel, and chromium chemistry of chert microbands pre-screened with in-situ analysis. Chemical Geology, **285**(1–4): 133–143. doi:10.1016/j.chemgeo.2011.03.019.

Bau, M. 1996. Controls on the fractionation of isovalent trace elements in magmatic and aqueous systems: Evidence from Y/Ho, Zr/Hf, and lanthanide tetrad effect. Contributions to Mineralogy and Petrology, **123**(3): 323–333. doi:10.1007/s004100050159.

Bau, M. 1999. Scavenging of dissolved yttrium and rare earths by precipitating iron oxyhydroxide: Experimental evidence for Ce oxidation, Y–Ho factionation, and lanthanide tetrad effect. Geochimica et Cosmochimica Acta, **63**(1): 67–77. doi:10.1016/S0016-7037(99)00014-9.

Bau, M., and Dulski, P. 1996. Distribution of yttrium and rare-earth elements in the Penge and Kuruman iron-formations, Transvaal Supergroup, South Africa. Precambrian Research, **79**(1–2): 37–55. doi:10.1016/0301-9268(95)00087-9.

Bau, M., and Dulski, P. 1999. Comparing yttrium and rare earths in hydrothermal fluids from the Mid-Atlantic Ridge: implications for

Y and REE behaviour during near-vent mixing and for the Y/Ho ratio of Proterozoic seawater. Chemical Geology, **155**(1–2): 77–90. doi:10.1016/S0009-2541(98)00142-9.

Bekker, A., Slack, J.F., Planavsky, N., Krapež, B., Hofmann, A., Konhauser, K.O., and Rouxel, O.J. 2010. Iron formation: The sedimentary product of a complex interplay among mantle, tectonic, oceanic, and biospheric processes. Economic Geology and the Bulletin of the Society of Economic Geologists, **105**(3): 467–508. doi:10.2113/gsecongeo.105.3.467.

Beukes, N.J., and Gutzmer, J. 2008. Origin and paleoenvironmental significance of major iron formations at the Archean–Paleoproterozoic boundary. Reviews in Economic Geology, **15**: 5–47.

Beukes, N.J., and Klein, C. 1992. Models for iron-formation deposition. *In* The Proterozoic biosphere: a multidisciplinary approach. *Edited by* J.W. Schopf and C. Klein. Cambridge University Press, Cambridge, UK. pp. 147–151.

Bolhar, R., Kamber, B.S., Moorbath, S., Fedo, C.M., and Whitehouse, M.J. 2004. Characterisation of early Archaean chemical sediments by trace element signatures. Earth and Planetary Science Letters, **222**(1): 43–60. doi:10.1016/j.epsl.2004.02.016.

Canfield, D.E. 1998. A new model for Proterozoic ocean chemistry. Nature, **396**(6710): 450–453. doi:10.1038/24839.

Canfield, D.E., Poulton, S.W., Knoll, A.H., Narbonne, G.M., Ross, G., Goldberg, T., and Strauss, H. 2008. Ferruginous conditions dominated later Neoproterozoic deep-water chemistry. Science, **321**(5891): 949–952. doi:10.1126/science.1154499. PMID:18635761.

Crowe, S.A., Fowle, D.A., Katsev, S., Sundby, B., Mucci, A., and Haffner, G.D. 2008*a*. Geochemistry of Mo in a modern Archean ocean analogue. Geochimica et Cosmochimica Acta, **72**: A190

Crowe, S.A., Jones, C., Katsev, S., Magen, C., O'Neill, A.H., Sturm, A., et al. 2008*b*. Photoferrotrophs thrive in an Archean ocean analogue. Proceedings of the National Academy of Sciences of the United States of America, **105**(41): 15938–15943. doi:10.1073/pnas.0805313105. PMID:18838679.

Cruse, A.M., and Lyons, T.W. 2004. Trace metal records of regional paleoenvironmental variability in Pennsylvanian (Upper Carboniferous) black shales. Chemical Geology, **206**(3–4): 319–345. doi:10.1016/j.chemgeo.2003.12.010.

De Carlo, E.H., and Green, W.J. 2002. Rare earth elements in the water column of Lake Vanda, McMurdo Dry Valleys, Antarctica. Geochimica et Cosmochimica Acta, **66**(8): 1323–1333. doi:10.1016/S0016-7037(01)00861-4.

Derry, L.A., and Jacobsen, S.B. 1990. The chemical evolution of Precambrian seawater: Evidence from REEs in banded iron formations. Geochimica et Cosmochimica Acta, **54**(11): 2965–2977. doi:10.1016/0016-7037(90)90114-Z.

Eggins, S.M., Woodhead, J.D., Kinsley, L.P.J., Mortimer, G.E., Sylvester, P., McCulloch, M.T., Hergt, J.M., and Handler, M.R. 1997. A simple method for the precise determination of > = 40 trace elements in geological samples by ICPMS using enriched isotope internal standardisation. Chemical Geology, **134**(4): 311–326. doi:10.1016/S0009-2541(96)00100-3.

Eisbacher, G.H. 1976. Proterozoic Rapitan Group and Related Rocks, Redstone River Area, District of Mackenzie. Geological Survey of Canada Paper 76. pp. 117–125.

Eisbacher, G.H. 1978. Re-definition and subdivision of the Rapitan Group, Mackenzie Mountains. Geological Survey of Canada Paper 77. pp. 1–21.

Eisbacher, G.H. 1981*a*. Late Precambrian tillites of the northern Yukon – Northwest Territories region, Canada. *In* Earth's pre-Pleistocene glacial record. *Edited by* M.J. Hambrey and W.B. Harland. Cambridge University Press, Cambridge, UK. pp. 724–727.

Eisbacher, G.H. 1981*b*. Sedimentary tectonics and glacial record in the Windermere Supergroup, Mackenzie Mountains, Northwestern Canada. Geological Survey of Canada Paper 80. pp. 1–41.

Eisbacher, G.H. 1985. Late Proterozoic rifting, glacial sedimentation, and sedimentary cycles in the light of Windermere deposition, western Canada. Palaeogeography, Palaeoclimatology, Palaeoecology, **51**(1–4): 231–254. doi:10.1016/0031-0182(85)90087-2.

Elderfield, H., Upstill-Goddard, R., and Sholkovitz, E.R. 1990. The rare earth elements in rivers, estuaries, and coastal seas and their significance to the composition of ocean waters. Geochimica et Cosmochimica Acta, **54**(4): 971–991. doi:10.1016/0016-7037(90)90432-K.

Eyles, N. 2008. Glacio-epochs and the supercontinent cycle after ~3.0 Ga: tectonic boundary conditions for glaciation. Palaeogeography, Palaeoclimatology, Palaeoecology, **258**(1–2): 89–129. doi:10.1016/j.palaeo.2007.09.021.

Farquhar, J., Wu, N., Canfield, D.E., and Oduro, H. 2010. Connections between sulfur cycle evolution, sulfur isotopes, sediments, an base metal sulfide deposits. Economic Geology and the Bulletin of the Society of Economic Geologists, **105**(3): 509–533. doi:10.2113/gsecongeo.105.3.509.

Fischer, W.W., and Knoll, A.H. 2009. An iron shuttle for deepwater silica in Late Archean and early Paleoproterozoic iron formation. Geological Society of America Bulletin, **121**: 222–235.

Frei, R., Gaucher, C., Poulton, S.W., and Canfield, D.E. 2009. Fluctuations in Precambrian atmospheric oxygenation recorded by chromium isotopes. Nature, **461**(7261): 250–253. doi:10.1038/nature08266. PMID:19741707.

Goldberg, T., Archer, C., Vance, D., and Poulton, S.W. 2009. Mo isotope fractionation during adsorption to Fe (oxyhydr)oxides. Geochimica et Cosmochimica Acta, **73**(21): 6502–6516. doi:10.1016/j.gca.2009.08.004.

Green, L.H., and Godwin, C.I. 1963. Mineral Industry of Yukon Territory and southwestern District of Mackenzie, 1962. Geological Survey of Canada Paper 63. pp. 15–18.

Helmstaedt, H., Eisbacher, G.H., and McGregor, J.A. 1979. Copper mineralization near an intra-Rapitan unconformity, Nite copper prospect, Mackenzie Mountains, Northwest Territories, Canada. Canadian Journal of Earth Sciences, **16**(1): 50–59. doi:10.1139/e79-005.

Helz, G.R., Bura-Nakić, E., Mikac, N., and Ciglenečki, I. 2011. New model for molybdenum behavior in euxinic waters. Chemical Geology, **284**(3–4): 323–332. doi:10.1016/j.chemgeo.2011.03.012.

Hoffman, P.F. 2009. Pan-glacial — a third state in the climate system. Geology Today, **25**(3): 100–107. doi:10.1111/j.1365-2451.2009.00716.x.

Hoffman, P.F., and Li, Z.X. 2009. A paleogeographic context for Neoproterozoic glaciation. Palaeogeography, Palaeoclimatology, Palaeoecology, **277**(3–4): 158–172. doi:10.1016/j.palaeo.2009.03.013.

Hoffman, P.F., Kaufman, A.J., Halverson, G.P., and Schrag, D.P. 1998. A Neoproterozoic snowball earth. Science, **281**(5381): 1342–1346. doi:10.1126/science.281.5381.1342. PMID:9721097.

Hofmann, H.J., Narbonne, G.M., and Aitken, J.D. 1990. Ediacaran remains from intertillite beds in northwestern Canada. Geology, **18**(12): 1199–1202. doi:10.1130/0091-7613(1990)018<1199:ERFIBI>2.3.CO;2.

Isley, A.E. 1995. Hydrothermal plumes and the delivery of iron to banded iron-formation. The Journal of Geology, **103**(2): 169–185. doi:10.1086/629734.

Isley, A.E., and Abbott, D.H. 1999. Plume-related mafic volcanism and the deposition of banded iron formation. Journal of Geophysical Research, **104**(B7): 15461–15477. doi:10.1029/1999JB900066.

James, N.P., Narbonne, G.M., and Kyser, T.K. 2001. Late Neoproterozoic cap carbonates: Mackenzie Mountains, northwestern Canada: precipitation and global glacial meltdown. Canadian Journal of Earth Sciences, **38**(8): 1229–1262. doi:10.1139/e01-046.

Jefferson, C.W., and Parrish, R.R. 1989. Late Proterozoic stratigraphy, U–Pb zircon ages, and rift tectonics, Mackenzie Mountains, northwestern Canada. Canadian Journal of Earth Sciences, **26**(9): 1784–1801. doi:10.1139/e89-151.

Jefferson, C.W., and Ruelle, J.C.L. 1987. The late Proterozoic Redstone copper belt. *In* Mineral deposits of the northern Cordillera. *Edited by* J.A. Morin. Canadian Institute of Mining and Metallurgy, West Mount, Que. Special Vol. 37. pp. 154–168.

Johannesson, K.H., Lyons, W.B., Graham, E.Y., and Welch, K.A. 2000. Oxyanion concentrations in eastern Sierra Nevada Rivers 3. Boron, molybdenum, vanadium, and tungsten. Aquatic Geochemistry, **6**(1): 19–46. doi:10.1023/A:1009622219482.

Johannesson, K.H., Hawkins, D.L., Jr, and Cortes, A. 2006. Do Archean chemical sediments record ancient seawater rare earth element patterns? Geochimica et Cosmochimica Acta, **70**(4): 871–890. doi:10.1016/j.gca.2005.10.013.

Johnston, D.T., Poulton, S.W., Dehler, C., Porter, S., Husson, J., Canfield, D.E., and Knoll, A.H. 2010. An emerging picture of Neoproterozoic ocean chemistry: Insights from the Chuar Group, Grand Canyon, USA. Earth and Planetary Science Letters, **290**(1–2): 64–73. doi:10.1016/j.epsl.2009.11.059.

Kamber, B.S. 2009. Geochemical fingerprinting: 40 years of analytical development and real world applications. Applied Geochemistry, **24**(6): 1074–1086. doi:10.1016/j.apgeochem.2009.02.012.

Kamber, B.S. 2010. Archean mafic–ultramafic volcanic landmasses and their effect on ocean atmosphere chemistry. Chemical Geology, **274**(1–2): 19–28. doi:10.1016/j.chemgeo.2010.03.009.

Kamber, B.S., Bolhar, R., and Webb, G.E. 2004. Geochemistry of late Archean stromatolites from Zimbabwe: evidence for microbial life in restricted epicontinental seas. Precambrian Research, **132**(4): 379–399. doi:10.1016/j.precamres.2004.03.006.

Kamber, B.S., Greig, A., and Collerson, K.D. 2005. A new estimate for the composition of weathered young upper continental crust from alluvial sediments, Queensland, Australia. Geochimica et Cosmochimica Acta, **69**(4): 1041–1058. doi:10.1016/j.gca.2004.08.020.

Kato, Y., Yamaguchi, K.E., and Ohmoto, H. 2006. Rare earth elements in Precambrian banded iron formations: secular changes of Ce and Eu anomalies and evolution of atmospheric oxygen. *In* GSA Memoir 198: evolution of earth's atmosphere, hydrosphere, and biosphere — constraints from ore deposits. *Edited by* S.E. Kesler and H. Ohmoto. The Geological Society of America, Boulder, Colo. pp. 269–289.

Keele, J. 1906. Upper Stewart River region, Yukon. Geological Survey of Canada Annual Report 1904. pp. 5–23.

Keele, J. 1910. Reconnaissance across the Mackenzie Mountains on the Pelly, Ross, and Gravel Rivers, Yukon and Northwest Territories. Geological Survey of Canada Report No 1097.

Kianian, M., and Khakzad, A. 2008. Geochemistry of glacigenic Neoproterozoic banded iron formations from the Kerma District (Iran). *In* Proceedings of the 33rd International Geological Congress, Oslo, Norway, 6–14 August 2008. International Geological Congress, Oslo, Norway. Session CGC-04.

Kirschvink, J.L. 1992. Late Proterozoic low-latitude global glaciation: the snowball earth. The Proterozoic biosphere: a multidisciplinary study. *Edited by* J.W. Schopf and C. Klein. Cambridge University Press, Cambridge, UK. pp. 51–52.

Klein, C., and Beukes, N.J. 1993. Sedimentology and geochemistry

of the glaciogenic late Proterozoic Rapitan iron-formation in Canada. Economic Geology and the Bulletin of the Society of Economic Geologists, **88**(3): 542–565. doi:10.2113/gsecongeo.88. 3.542.

Klein, C., and Ladeira, E.A. 2004. Geochemistry and mineralogy of Neoproterozoic banded iron-formations and some selected, silicieous manganese formations form the Urucum District, Mato Grosso Do Sul, Brazil. Economic Geology and the Bulletin of the Society of Economic Geologists, **99**(6): 1233–1244. doi:10.2113/ 99.6.1233.

Kletzin, A., and Adams, M.W.W. 1996. Tungsten in biological systems. FEMS Microbiology Reviews, **18**(1): 5–63. doi:10.1111/ j.1574-6976.1996.tb00226.x. PMID:8672295.

Konhauser, K.O., Pecoits, E., Lalonde, S.V., Papineau, D., Nisbet, E.G., Barley, M.E., et al. 2009. Oceanic nickel depletion and a methanogen famine before the Great Oxidation Event. Nature, **458**(7239): 750–753. doi:10.1038/nature07858. PMID:19360085.

Kump, L.R., and Seyfried, W.E., Jr. 2005. Hydrothermal Fe fluxes furing the Precambrian: effect of low oceanic sulfate concentration and low hydrostatic pressure on the composition of black smokers. Earth and Planetary Science Letters, **235**(3–4): 654–662. doi:10. 1016/j.epsl.2005.04.040.

Lawrence, M.G., and Kamber, B.S. 2006. The behaviour of the rare earth elements during estuarine mixing-revisited. Marine Chemistry, **100**(1–2): 147–161. doi:10.1016/j.marchem.2005.11.007.

Lawrence, M.G., Greig, A., Collerson, K.D., and Kamber, B.S. 2006. Rare earth element and yttrium variability in South East Queensland waterways. Aquatic Geochemistry, **12**(1): 39–72. doi:10. 1007/s10498-005-4471-8.

Li, C., Love, G.D., Lyons, T.W., Fike, D.A., Sessions, A.L., and Chu, X. 2010. A stratified redox model for the Ediacaran ocean. Science, **328**(5974): 80–83. doi:10.1126/science.1182369. PMID: 20150442.

Long, D.G.F., Rainbird, R.H., Turner, E.C., and MacNaughton, R.B. 2008. Early Neoproterozoic strata (sequence B) of mainland northern Canada and Victoria and Banks islands: a contribution to the Geological Atlas of the North Canadian Mainland Sedimentary Basin. Geological Survey of Canada, Open File 5700. 24 pp.

Lottermoser, B.G., and Ashley, P.M. 2000. Geochemistry, petrology and origin of Neoproterozoic ironstones in the eastern part of the Adelaide Geosyncline, South Australia. Precambrian Research, **101**(1): 49–67. doi:10.1016/S0301-9268(99)00098-4.

Lyons, T.W., Werne, J.P., Hollander, D.J., and Murray, R.W. 2003. Contrasting sulfur geochemistry and Fe/Al and Mo/Al ratios across the last oxic-to-anoxic transition in the Cariaco Basin, Venezuela. Chemical Geology, **195**(1–4): 131–157. doi:10.1016/ S0009-2541(02)00392-3.

Macdonald, F.A., Schmitz, M.D., Crowley, J.L., Roots, C.F., Jones, D.S., Maloof, A.C., et al. 2010a. Calibrating the Cryogenian. Science, **327**(5970): 1241–1243. doi:10.1126/science.1183325. PMID:20203045.

Macdonald, F.A., Strauss, J.V., Rose, C.V., Dudás, F.Ö., and Schrag, D.P. 2010b. Stratigraphy of the Port Nolloth Group of Namibia and South Africa and implications for the age of Neoproterozoic iron formations. American Journal of Science, **310**(9): 862–888. doi:10.2475/09.2010.05.

Marx, S.K., and Kamber, B.S. 2010. Trace-element systematics of sediments in the Murray–Darling Basin, Australia: sediment provenance and palaeoclimate implications of fine scale heterogeneity. Applied Geochemistry, **25**(8): 1221–1237. doi:10.1016/j. apgeochem.2010.05.007.

Meyer, E.E., Burgreen, B.N., Lackey, H., Landis, J.D., Quicksall, A.N., and Bostick, B.C. 2008. Evidence for basin restiction during syn-collisional basin formation in the Silurian Arisaig Group,

Nova Scotia. Chemical Geology, **256**(1–2): 1–11. doi:10.1016/j. chemgeo.2008.06.016.

Mikucki, J.A., Pearson, A., Johnston, D.T., Turchyn, A.V., Farquhar, J., Schrag, D.P., et al. 2009. A contemporary microbially maintained subglacial ferrous "ocean". Science, **324**(5925): 397–400. doi:10.1126/science.1167350. PMID:19372431.

Morford, J.L., and Emerson, S. 1999. The geochemistry of redox sensitive trace metals in sediments. Geochimica et Cosmochimica Acta, **63**(11–12): 1735–1750. doi:10.1016/S0016-7037(99)00126-X.

Morford, J.L., Emerson, S.R., Breckel, E.J., and Kim, S.H. 2005. Diagenesis of oxyanions (V, U, Re, and Mo) in pore waters and sediments from a continental margin. Geochimica et Cosmochimica Acta, **69**(21): 5021–5032. doi:10.1016/j.gca.2005.05.015.

Narbonne, G.M., and Aitken, J.D. 1995. Neoproterozoic of the Mackenzie Mountains, northwestern Canada. Precambrian Research, **73**(1–4): 101–121. doi:10.1016/0301-9268(94)00073-Z.

Nothdurft, L.D., Webb, G.E., and Kamber, B.S. 2004. Rare earth element geochemistry of Late Devonian reefal carbonate, Canning Basin, Western Australia: confirmation of a seawater REE proxy in ancient limestones. Geochimica et Cosmochimica Acta, **68**(2): 263–283. doi:10.1016/S0016-7037(03)00422-8.

Ohta, A., Ishii, S., Sakakibara, M., Mizuno, A., and Kawabe, I. 1999. Systematic correlation of the Ce anomaly with the Co/(Ni + Cu) ratio and Y fractionation from Ho in distinct types of Pacific deep-sea nodules. Geochemical Journal, **33**(6): 399–417. doi:10.2343/ geochemj.33.399.

Pattan, J.N., and Pearce, N.J.G. 2009. Bottom water oxygenation history in southeastern Arabian Sea during the past 140 ka: results from redox-sensitive elements. Palaeogeography, Palaeoclimatology, Palaeoecology, **280**(3–4): 396–405. doi:10.1016/j.palaeo. 2009.06.027.

Pecoits, E., Gingras, M., Aubet, N., and Konhauser, K. 2008. Ediacaran in Uruguay: palaeoclimatic and palaeobiological implications. Sedimentology, **55**(3): 689–719. doi:10.1111/j. 1365-3091.2007.00918.x.

Picard, S., Lécuyer, C., Barrat, J.-A., Garcia, J.P., Dromart, G., and Sheppard, S.M.F. 2002. Rare-earth element contents of Jurassic fish and reptile teeth and their potential relation to seawater composition (Anglo-Paris basin, France and England). Chemical Geology, **186**(1–2): 1–16. doi:10.1016/S0009-2541(01)00424-7.

Planavsky, N., Bekker, A., Rouxel, O.J., Kamber, B., Hofmann, A., Knudsen, A., and Lyons, T.W. 2010a. Rare earth element and yttrium compositions of Archean and Paleoproterozoic Fe formations revisited: new perspectives on the significance and mechanisms of deposition. Geochimica et Cosmochimica Acta, **74**(22): 6387–6405. doi:10.1016/j.gca.2010.07.021.

Planavsky, N., Rouxel, O.J., Bekker, A., Lalonde, S.V., Konhauser, K.O., Reinhard, C.T., and Lyons, T.W. 2010b. The evolution of the marine phosphate reservoir. Nature, **467**(7319): 1088–1090. doi:10.1038/nature09485. PMID:20981096.

Pollack, G.D., Krogstad, E.J., and Bekker, A. 2009. U–Th–Pb–REE systematics of organic-rich shales from the ca. 2.15 Ga Sengoma Argillite Formation, Botswana: evidence for oxidative continental weathering during the Great Oxidation Event. Chemical Geology, **260**(3–4): 172–185. doi:10.1016/j.chemgeo.2008.10.038.

Poulton, S.W., and Canfield, D.E. 2011. Ferruginous conditions: a dominant feature of the ocean through earth's history. Elements, **7** (2): 107–112. doi:10.2113/gselements.7.2.107.

Poulton, S.W., Fralick, P.W., and Canfield, D.E. 2004. The transition to a sulphidic ocean ~1.84 billion years ago. Nature, **431**(7005): 173–177. doi:10.1038/nature02912.

Poulton, S.W., Fralick, P.W., and Canfield, D.E. 2010. Spatial variability in oceanic redox structure 1.8 billion years ago. Nature Geoscience, **3**(7): 486–490. doi:10.1038/ngeo889.

Pufahl, P.K., Hiatt, E.E., and Kyser, T.K. 2010. Does the Paleoproterozoic Animikie Basin record the sulfidic ocean transition? Geology, **38**(7): 659–662. doi:10.1130/G30747.1.

Raiswell, R., Tranter, M., Benning, L.G., Siegert, M., De'ath, R., Huybrechts, P., and Payne, T. 2006. Contributions from glacially derived sediment to the global iron (oxyhydr)oxide cycle: implications for iron delivery to the oceans. Geochimica et Cosmochimica Acta, **70**(11): 2765–2780. doi:10.1016/j.gca.2005.12.027.

Rose, A.W., Smith, A.T., Lustwerk, R.L., Ohmoto, H., and Hoy, L.D. 1986. Geochemical aspects of stratiform and red-bed copper deposits in the Catskill Formation (Pennsylvania, USA) and Redstone Area (Canada). Sequence of mineralization in sediment-hosted copper deposits (part 3). *In* Geology and metallogeny of copper deposits. *Edited by* G.H. Friedrich. Springer-Verlag, Berlin, Germany. pp. 414–421.

Ross, G.M., and Villeneuve, M.E. 1997. U–Pb geochronology of stranger stones in Neoproterozoic diamictites, Canadian Cordillera: implications for provenance and ages of deposition. Radiogenic age and isotopic studies: report 10. Geological Survey of Canada, Current Research 1997-F. pp. 141–155.

Scott, C., Lyons, T.W., Bekker, A., Shen, Y., Poulton, S.W., Chu, X., and Anbar, A.D. 2008. Tracing the stepwise oxygenation of the Proterozoic ocean. Nature, **452**(7186): 456–459. doi:10.1038/nature06811. PMID:18368114.

Seiler, R.L., Stollenwerk, K.G., and Garbarino, J.R. 2005. Factors controlling tungsten concentrations in ground water, Carson Desert, Nevada. Applied Geochemistry, **20**(2): 423–441. doi:10.1016/j.apgeochem.2004.09.002.

Shen, Y., Canfield, D.E., and Knoll, A.H. 2002. Middle Proterozoic ocean chemistry: evidence from the McArthur basin, Northern Australia. American Journal of Science, **302**(2): 81–109. doi:10.2475/ajs.302.2.81.

Shen, Y., Knoll, A.H., and Walter, M.R. 2003. Evidence for low sulphate and anoxia in a mid-Proterozoic marine basin. Nature, **423**(6940): 632–635. doi:10.1038/nature01651.

Shields, G.A., and Webb, G.E. 2004. Has the REE composition of seawater changed over geological time? Chemical Geology, **204**(1–2): 103–107. doi:10.1016/j.chemgeo.2003.09.010.

Shields-Zhou, G., and Och, L. 2011. The case for a Neoproterozoic oxygenation event: geochemical evidence and biological consequences. GSA Today, **21**(3): 4–11. doi:10.1130/GSATG102A.1.

Slack, J.F., Grenne, T., Bekker, A., Rouxel, O.J., and Lindberg, P.A. 2007. Suboxic deep seawater in the late Paleoproterozoic: evidence from hematitic chert and iron formation related to seafloor – hydrothermal sulfide deposits, central Arizona, USA. Earth and Planetary Science Letters, **255**(1–2): 243–256. doi:10.1016/j.epsl.2006.12.018.

Stuart, R.A. 1963. Geology of the Snake River iron deposit. DIAND Assessment Files, Yellowknife, N.W.T. 18 pp.

Taylor, S.R., and McLennan, S.M. 1985. The continental crust: its composition and evolution. Blackwell, Oxford, UK. p. 312.

Tribovillard, N., Riboulleau, A., Lyons, T., and Baudin, F. 2004. Enhanced trapping of molybdenum by sulfurized marine organic matter of marine origin in Mesozoic limestones and shales. Chemical Geology, **213**(4): 385–401. doi:10.1016/j.chemgeo.2004.08.011.

Tribovillard, N., Algeo, T.J., Lyons, T., and Riboulleau, A. 2006. Trace metals as paleoredox and paleoproductivity proxies: an update. Chemical Geology, **232**(1–2): 12–32. doi:10.1016/j.chemgeo.2006.02.012.

Trompette, R., De Alvarenga, C.J.S., and Walde, D. 1998. Geological evolution of the Neoproterozoic Corumbá graben system (Brazil). Depositional context of the stratified Fe and Mn ores of the Jacadigo Group. Journal of South American Earth Sciences, **11**(6): 587–597. doi:10.1016/S0895-9811(98)00036-4.

Ulrich, T., Kamber, B.S., Jugo, P.J., and Tinkham, D.K. 2009. Imaging element-distribution patterns in minerals by laser ablation – inductively coupled plasma – mass spectrometry (LA–ICP–M.S.). Canadian Mineralogist, **47**(5): 1001–1012. doi:10.3749/canmin.47.5.1001.

Van der Weijden, C.H. 2002. Pitfalls of normalisation of marine geochemical data using a common divisor. Marine Geology, **184**(3–4): 167–187. doi:10.1016/S0025-3227(01)00297-3.

Webb, G.E., and Kamber, B.S. 2000. Rare earth elements in Holocene reefal microbialites: a new shallow seawater proxy. Geochimica et Cosmochimica Acta, **64**(9): 1557–1565. doi:10.1016/S0016-7037(99)00400-7.

Yeo, G.M. 1978. Iron-formation in the Rapitan Group, Mackenzie Mountains, Yukon and Northwest Territories. DIAND Mineral Industry Report 1975, NWT Economic Geology Series 1978-5. pp. 170–175.

Yeo, G.M. 1981. The late Proterozoic Rapitan glaciation in the northern Cordillera. *In* Proterozoic basins of Canada. *Edited by* F. H.A. Campbell. Geological Survey of Canada Paper 81-10. pp. 25–46.

Young, G.M. 1976. Iron-formation and glaciogenic rocks of the Rapitan Group, Northwest Territories, Canada. Precambrian Research, **3**(2): 137–158. doi:10.1016/0301-9268(76)90030-9.

Young, G.M. 1988. Proterozoic plate tectonics, glaciation and iron-formations. Sedimentary Geology, **58**(2–4): 127–144. doi:10.1016/0037-0738(88)90066-8.

Young, G.M. 1992. Late Proterozoic stratigraphy and the Canada–Australia connection. Geology, **20**(3): 215–218. doi:10.1130/0091-7613(1992)020<0215:LPSATC>2.3.CO;2.

Young, G.M. 2002. Stratigraphic and tectonic settings of Proterozoic glaciogenic rocks and banded iron-formations: relevance to the snowball earth debate. Journal of African Earth Sciences, **35**(4): 451–466. doi:10.1016/S0899-5362(02)00158-6.

Zhang, J., and Nozaki, Y. 1996. Rare earth elements and yttrium in seawater: ICP–M.S. determinations in the East Caroline, Coal Sea, and South Fiji basins of the western South Pacific Ocean. Geochimica et Cosmochimica Acta, **60**(23): 4631–4644. doi:10.1016/S0016-7037(96)00276-1.

Ziegler, P.A. 1959. Frühpaläozoiche Tillite im östlichen Yukon-Territorium (Kanada). Eclogae Geologicae Helvetiae, **52**(2): 735–741.